The Stellar Populations of Low Luminosity Active Galactic Nuclei. I: Ground Based Observations[1]

Roberto Cid Fernandes[1], Rosa M. González Delgado[2] Henrique Schmitt[3,10,11], Thaisa Storchi-Bergmann[4], Lucimara P. Martins[5,9], Enrique Pérez[2], Timothy Heckman[6,12], Claus Leitherer[5], & Daniel Schaerer[7,8]

(1) Depto. de Física-CFM, Universidade Federal de Santa Catarina, C.P. 476, 88040-900, Florianópolis, SC, Brazil (cid@astro.ufsc.br)

(2) Instituto de Astrofísica de Andalucia (CSIC), P.O. Box 3004, 18080 Granada, Spain (rosa@iaa.es; eperez@iaa.es)

(3) National Radio Astronomy Observatory, PO Box 0, Socorro, NM 87801 (hschmitt@nrao.edu)

(4) Instituto de Física, Universidad Federal do Rio Grande do Sul, C.P. 15001, 91501-970, Poto Alegre, RS, Brazil (thaisa@if.ufrgs.br)

(5) Space Telescope Institute, 3700 San Martin Drive, Baltimore, MD 21218, USA (martins@stsci.edu; leitherer@stsci.edu)

(6) Department of Physics & Astronomy, JHU, Baltimore, MD 21218 (heckman@pha.jhu.edu)

(7) Observatoire de Geneve, 51, Ch. des Maillettes, CH-1290 Sauverny, Switzerland

(8) Laboratoire d'Astrophysique,UMR 5572, 14 AV. E. Belin, F-31400 Toulouse, France

(9) Intituto de Astronomía, Geofísica e Ciencias Atmosféricas, 05508-900 Sao Paulo, Brazil

ABSTRACT

We present a spectroscopic study of the stellar populations of Low Luminosity Active Galactic Nuclei (LLAGN). Our main goal is to determine whether the stars

[10]Jansky Fellow

[11]Visiting Astronomer, Kitt Peak National Observatory, National Optical Astronomy Observatories, which are operated by AURA, Inc., under a cooperative agreement with the National Science Foundation.

[12]Also Adjunct Astronomer at STScI

who live in the innermost (100 pc-scale) regions of these galaxies are in some way related to the emission line properties, which would imply a link between the stellar population and the ionization mechanism. High signal to noise, ground based long-slit spectra in the 3500–5500 Å interval were collected for 60 galaxies: 51 LINERs and LINER/HII Transition Objects, 2 Starburst and 7 non-active galaxies. In this paper, first of a series, we (1) describe the sample; (2) present the nuclear spectra; (3) characterize the stellar populations of LLAGN by means of an empirical comparison with normal galaxies; (4) measure a set of spectral indices, including several absorption line equivalent widths and colors indicative of stellar populations; (5) correlate the stellar indices with emission line ratios which may distinguish between possible excitation sources for the gas.

Our main findings are: (1) Few LLAGN have a detectable young ($\lesssim 10^7$ yr) starburst component, indicating that very massive stars do not contribute significantly to the optical continuum. In particular, no features due to Wolf-Rayet stars were convincingly detected. (2) High Order Balmer absorption lines of HI (HOBLs), on the other hand, are detected in $\sim 40\%$ of LLAGN. These features, which are strongest in 10^8–10^9 yr intermediate age stellar populations, are accompanied by diluted metal absorption lines and bluer colors than other objects in the sample. (3) These intermediate age populations are very common ($\sim 50\%$) in LLAGN with relatively weak [OI] emission ([OI]/H$\alpha \leq 0.25$), but rare ($\sim 10\%$) in LLAGN with stronger [OI]. This is intriguing since LLAGN with weak [OI] have been previously hypothesized to be "transition objects" in which both an AGN and young stars contribute to the emission-line excitation. Massive stars, if present, are completely outshone by intermediate age and old stars in the optical. This happens in at least a couple of objects where independent UV spectroscopy detects young starbursts not seen in the optical. (4) Objects with predominantly old stars span the whole range of [OI]/Hα values, but (5) sources with significant young and/or intermediate age populations are nearly all ($\sim 90\%$) weak [OI] emitters.

These new findings suggest a link between the stellar populations and the gas ionization mechanism. The strong-[OI] objects are most likely true LLAGN, with stellar processes being insignificant. However, the weak-[OI] objects may comprise two populations, one where the ionization is dominated by stellar processes and another where it is either governed by an AGN or by a more even mixture of stellar and AGN processes. Possible stellar sources for the ionization include weak starbursts, supernova-remnants and evolved post-starburst populations. These scenarios are examined and constrained by means of complementary observations and detailed modeling of the stellar populations in forthcoming communications.

Subject headings: galaxies:active – galaxies:nuclei – galaxies:stellar populations – galaxies:star formation

1. Introduction

Low Ionization Nuclear Emission-line Regions, better known as LINERs, were first described as a separate class of galaxies by Heckman (1980). These objects have characteristically strong low-ionization forbidden lines of [OI], [NII], [SII] and [OII] that distinguish them from both Seyfert and Starburst nuclei. Because of their small luminosities compared to Seyferts and quasars, these objects are often called Low Luminosity Active Galactic Nuclei (LLAGN). LLAGN are the most common form of nuclear activity in the local universe. In the magnitude limited survey by Ho, Filippenko & Sargent (1995, 1997, hereafter HFS97), they comprise $\sim 1/3$ of all galaxies.

What powers LLAGN and how do they fit in the global picture of AGN? Are they all truly "dwarf Seyferts" powered by accretion onto nearly-dormant supermassive black holes ("dead QSOs") or can some of them be explained at least partly in terms of stellar process?

These questions have been at the forefront of AGN research for over two decades. Nowadays there is no doubt that a substantial fraction of these nuclei contain *bona fide* AGN. Among the most solid evidence in support of this "AGN model" is the fact that $\sim 1/5$ of LLAGN have broad (few thousand km/s) Hα emission (HFS97), signaling the presence of a Broad Line Region, a hallmark of AGN. In fact, some of the most compelling evidence for the existence of nuclear accretion disks come from LLAGN with double-peaked broad Balmer lines (eg, NGC 1097, Storchi-Bergmann et al. 1997; M81, Bower et al. 1996). X-ray observations (Terashima et al. 2000; Ho et al. 2001) and the detection of compact nuclear radio emission (Falcke et al. 2000; Nagar et al. 2000) also support the AGN model. Similarities between LLAGN and Seyferts were also identified in the properties of their host galaxies (Ho, Filippenko & Sargent 2003). In the theoretical front, it has long been known that photoionization by a typical AGN can reproduce the characteristic LINER emission line spectrum (Ferland & Netzer 1983; Halpern & Steiner 1983). These and other evidence

[1]Based on observations made with the Nordic Optical Telescope, operated on the island of La Palma jointly by Denmark, Finland, Iceland, Norway, and Sweden, in the Spanish Observatorio del Roque de los Muchachos of the Instituto de Astrofísica de Canárias.

(see Barth 2002 and references therein) have contributed to the general understanding that many, maybe most LLAGN are *bona fide* members of the AGN family, the low luminosity cousins of Seyferts.

Despite this general consensus, for nearly as long as LINERs have existed in the literature, it has been suspected that they constitute a rather mixed bag of phenomena (e.g., Filippenko 1996; Heckman 1996). LINER-like spectra are known to occur in as diverse environments as cluster cooling flows (e.g. Heckman et al. 1989; Donahue & Voit 1991), starburst driven super-winds (Heckman, Armus, & Miley 1990), and the bulges of early-type galaxies (e.g. Heckman 1996) besides the nuclei of galaxies. It is therefore likely that a variety of ionization mechanisms are capable of producing a LINER-type spectrum, and indeed several models not involving photoionization by an AGN have been proposed to explain the emission line characteristics of these objects. Among them are shocks (Heckman 1980; Dopita & Sutherland 1995), which may be associated with SN remnants, photoionization by unusually hot young stars (Filippenko & Terlevich 1992; Shields 1992; Barth & Shields 2000), or by post-AGB stars (Binette et al. 1994; Taniguchi, Shioya & Murayama 2000). Even in nuclei where an AGN is conclusively known to exist, it is unclear what is its role in the gas ionization and in the overall energetics, since the AGN may coexist with one or more of these other ionizing agents. For instance, CIV and SiIV PCygni lines from O stars were detected in the space-UV for a few LLAGN by Maoz et al. (1998), lending support to the idea that at least some of these objects may be powered by young stars. Yet, in some of these same nuclei, like NGC 4569 and NGC 4594, an AGN has been detected by Chandra observations (Ho et al. 2001). These nuclei therefore contain both a compact starburst and an AGN. NGC 4303, recently studied by Colina et al. (2002) and Jiménez-Bailon et al. (2003) is another example. This coexistence of a starburst and an AGN is reminiscent of the starburst + Seyfert 2 composites discussed by Heckman et al. (1997), González Delgado et al. (1998), Storchi-Bergmann, Cid Fernandes & Schmitt (1998), González Delgado, Heckman & Leitherer (2001), Cid Fernandes et al. (2001a) and Joguet et al. (2001).

The question then arises of what are the relative roles of accretion and other processes in the energetics of LLAGN, and how to segregate nuclei where accretion is the dominant energy source from those whose emission lines are powered mainly by stars or their remnants. HFS97 addressed this issue by dividing LLAGN into two subclasses: "pure" or "normal" LINERs and LINER/HII "Transition Objects" (hereafter TOs), whose emission line ratios are intermediate between those of LINERs and HII regions. The fundamental distinction between LINERs and TOs is the relative strength of the [OI]λ6300 line (e.g. [OI]/Hα). This collisionally-excited line arises in warm neutral gas, and as such is weak in gas that is photoionized by the soft radiation from O stars, since the transition between the external cold neutral gas and internal ionized layers is very sharp. In contrast, an AGN produces

highly energetic photons that penetrate deeply into (and heat) the neutral gas. Although useful, the division of LLAGN onto LINERs and TOs is largely arbitrary, given that there is no clear-cut gap between LINERs and HII nuclei in the [OI]/Hα ratio.

The idea when the TO class was introduced was, in the words of HFS97, that "TOs can be most naturally explained as normal LINERs whose integrated spectra are diluted or contaminated by neighboring HII regions" (see also Ho, Filippenko & Sargent 1993; Gonçalvez, Véron & Véron-Cetty 1999). Accordingly, the most popular models for these sources involve photoionization by hot stars in a weak nuclear starburst (Shields 1992; Filippenko & Terlevich 1992; Barth & Shields 2000), although mechanical heating by supernovae following a short-duration burst (Engelbracht et al. 1998; Alonso Herrero et al. 2000) and photoionization by evolved "post-starburst" populations (Taniguchi et al. 2000) have also been invoked to explain their emission line properties.

Given that so many different mechanisms are capable of producing a similar emission line spectrum, it is evident that emission line data *per se* will not be able to distinguish between different models.

In this paper and others in this series we examine the stellar populations in a sample of LLAGN in search for clues of their nature. A simple motivation for this is that all alternative non-AGN models discussed above share a common trait: They all involve stars in one way or another, be they young and massive (a starburst), older and not so massive (post-starburst models) or massive but dead (SNR shocks). Characterizing the stellar populations of LLAGN may thus provide us with the extra information needed to assess the relevance of the proposed scenarios.

With this central goal in mind, we have carried out a spectroscopic survey of LINERs and TOs in the 3500–5500 Å interval. This spectral range contains several stellar population features of interest, including the WR bump at 4680 Å (an unambiguous signpost of the presence of young, $< 10^7$ yr massive stars), high order Balmer absorption lines (HOBLs) of HI (which signal the presence of evolved starbursts, from 10^7 up to 10^9 yr), the 4000 Å break, the Balmer jump and several metal lines typical of old populations, such as CaII K, the G-band and others. A detailed scrutiny of these features by means of stellar population analysis provides a *direct* test of models proposed for LINERs and TOs. This technique can be contrasted to the mostly used *indirect* approach of comparing emission line ratios with predictions from photoionization or shock models.

Our survey is based on the sample of HFS97, but differs from it in two important aspects: Wavelength coverage and spatial resolution. Unlike HFS97 we do not reach the red part of the spectrum, which includes emission lines which are the basis of spectral classification. On

the other hand, the HFS97 spectra start at 4230 Å, whereas our data goes down to 3500 Å. This near-UV edge contains several key stellar population diagnostics (like the HOBLs) which have not been systematically studied in previous LLAGN surveys. As shown here, results obtained in this spectral range give us a new perspective on the nature of these galaxies.

In this paper we concentrate in the presentation of the data. Companion papers will discuss stellar population synthesis analysis (González Delgado et al. 2003, hereafter Paper II), spatial gradients of spectral properties, morphology, emission line properties and models. This paper is organized as follows: In §**??** and §**??** we describe the sample, observations and reduction process. In §**??** the nuclear spectra are presented. A suite of properties has been measured from these spectra, such as equivalent widths and colors. These are presented in §**??**, which also compares our measurements with previously published results. This section also presents an objective definition of the pseudo continuum used to measure stellar population indices in Bica's system. In §**??** we examine the most important finding of this investigation: The strong connection between stellar population and emission line properties in LLAGN. Finally, §**??** summarizes our results.

2. Sample

We selected galaxies from the Ho et al. (1995, 1997) sample for this study because it is the most complete and homogeneous survey of LLAGN available and provides a representative population of galaxies in the local universe. HFS97 divided LLAGN into two subclasses: "pure" or "normal" LINERs and LINER/HII "Transition Objects" (TOs), whose emission line ratios are intermediate between those of LINERs and HII regions. Some Seyfert galaxies also match the usual definition of LLAGN, $L_{H\alpha} < 10^{40}$ erg s^{-1}, but in this paper "LLAGN" is used as a synonimous for LINERs and TOs. HFS97 distinguish LINERs from TOs by the value of the [OI]λ6300/Hα emission line ratio: They define LINERs as nuclei with [OI]/H$\alpha \geq 0.17$, while for TOs $0.08 \leq$ [OI]/H$\alpha < 0.17$. Because of its sensitivity to the high energy part of the ionizing spectrum, the [OI]/Hα ratio is a good indicator of the presence of an AGN.

LINERs and TOs are further distinguished from Seyfert and HII nuclei on the basis of other line ratios: [OIII]λ5007/H$\beta < 3$, [NII]λ6583/H$\alpha \geq 0.6$ and [SII]$\lambda\lambda$6716, 6731/H$\alpha \geq$ 0.4. According to these criteria, the HFS97 survey contains 94 LINERs and 65 TOs. We have added three other galaxies to these lists: NGC 772 (classified as "H/T2:" by HFS97, ie, a hybrid between an HII nucleus and a TO) and NGC 2685 (a "S2/T2:") were grouped among TOs, while NGC 6951 (classified as a Seyfert 2 by HFS97 and as a Seyfert 2/LINER

by Perez et al. 2000) was grouped among LINERs. With these additions the HFS survey contains 162 LLAGN. This sample will hereafter be called the "HFS sample".

We have observed a subset of 28 LINERs and 23 TOs, which corresponds to $\sim 1/3$ of the HFS sample. For comparison purposes, we also observed 7 normal galaxies and 2 Starburst nuclei, which gives a total of 60 galaxies. Table **??** lists the galaxies in our sample, along with several properties extracted from HFS97. As in HFS97, LINERs are listed as either L2 (if they contain only narrow lines) or L1.9 (if a broad Hα was detected), and similarly for TOs. The L2/T2 and T2/L2 mixed-classes are used when a galaxy looks more like a LINER than like a TO and vice-versa, respectively. These ambiguous cases arise due to inconsistencies between the classification implied by different line ratios and measurements uncertainties. About 13% of the LINERs and TOs in the HFS sample are in these ambiguous categories (and many more have uncertain classifications), which shows that the frontier between LINERs and TOs is a rather fuzzy one.

2.1. LINERs, TOs, weak and strong-[OI] nuclei: classification issues

In this paper we will adopt a slightly different classification criterion for LLAGN. While HFS97 divide LINERs from TOs at [OI]/H$\alpha = 0.17$, we prefer to place this dividing line at 0.25. To avoid confusion, we shall refer to sources with [OI]/H$\alpha \leq 0.25$ as "weak-[OI] nuclei", while [OI]/H$\alpha > 0.25$ sources are classed "strong-[OI]". Our motivation to introduce these definitions is entirely empirical. We shall see that the [OI]/H$\alpha = 0.25$ limit represents much better the combined distributions of [OI]/Hα and stellar population properties in LLAGN. Clearly, this choice is largely irrelevant insofar as emission lines are concerned, since weak-[OI] nuclei still have [OI]/Hα values intermediate between strong-[OI] and HII nuclei. In other words, weak-[OI] nuclei are essentially TOs and strong-[OI] are all LINERs.

Of the 162 LLAGN in the HFS sample, 56 (35%) have [OI]/H$\alpha > 0.25$ and 106 (65%) have [OI]/H$\alpha \leq 0.25$. The corresponding fractions for our sample are nearly identical: 17 and 34 of our 51 LLAGN fit our definitions strong and weak-[OI] nuclei respectively.

2.2. Comparison with the HFS sample

Although we have drawn objects exclusively from the HFS sample, it is important to evaluate whether we have introduced any bias in our sample selection. In Figure 1 we compare the distributions of distances (d) and morphological types (T) in these two samples. Triangles and circles correspond to strong and weak-[OI] LLAGN respectively, and filled

Table 1. Sample Properties

Galaxy Name	Spectral Class	Hubble Type	T-type	v $km\,s^{-1}$	dist. Mpc	pc/″ pc	log $L_{H\alpha}$ $erg\,s^{-1}$	[OI]/Hα
NGC 266	L1.9	SB(rs)ab	2.0	4662	62.4	302	39.30	0.280c
NGC 315	L1.9	E+:	-4.0	4935	65.8	319	39.55	0.590
NGC 404	L2	SA(s)0-:	-3.0	-46	2.4	11	37.63	0.170
NGC 410	T2:	E+:	-4.0	5295	70.6	342	39.43	0.097u
NGC 428	L2/T2:	SAB(s)m	9.0	1160	14.9	72	36.98L	0.190u
NGC 521	T2/H:	SB(r)bc	4.0	5039	67.0	324	39.16	0.086c
NGC 660	T2/H:	SB(s)a pec	1.0	852	11.8	57	38.89	0.047
NGC 718	L2	SAB(s)a	1.0	1734	21.4	103	38.45	0.210
NGC 772[1]	H/T2:	SA(s)b	3.0	2458	32.6	158	39.24	0.026b
NGC 841	L1.9:	(R')SAB(s)ab	2.1	4539	59.5	288	39.11L	0.580b
NGC 1052	L1.9	E4	-5.0	1499	17.8	86	39.45r	0.710
NGC 1161	T1.9:	SA0	-2.0	1940	25.9	125	38.70	0.140u
NGC 1169	L2	SAB(r)b	3.0	2386	33.7	163	38.67	0.320
NGC 2681	L1.9	(R')SAB(rs)0/a	0.0	688	13.3	64	38.83L	0.190b
NGC 2685[2]	S2/T2:	(R)SB0+pec	-1.0	820	16.2	78	38.66	0.130b
NGC 2911	L2	SA(s)0: pec	-2.0	3183	42.2	204	39.38r	0.310
NGC 3166	L2	SAB(rs)0/a	0.0	1344	22.0	106	39.10	0.270
NGC 3169	L2	SA(s)a pec	1.0	1234	19.7	95	39.02	0.280
NGC 3226	L1.9	E2: pec	-5.0	1321	23.4	113	38.93	0.590
NGC 3245	T2:	SA(r)0?	-2.0	1348	22.2	107	39.59	0.086c
NGC 3627	T2/S2	SAB(s)b	3.0	727	6.6	31	38.50	0.130
NGC 3705	T2	SAB(r)ab	2.0	1018	17.0	82	38.66	0.079b
NGC 4150	T2	SA(r)0?	-2.0	43	9.7	47	38.18	0.130
NGC 4192	T2	SAB(s)ab	2.0	-142	16.8	81	38.97	0.140
NGC 4438	L1.9	SA(s)0/a:	0.0	64	16.8	81	39.37	0.270
NGC 4569	T2	SAB(rs)ab	2.0	-235	16.8	81	40.28r	0.062
NGC 4736	L2	(R)SA(r)ab	2.0	307	4.3	20	37.81r	0.240
NGC 4826	T2	(R)SA(rs)ab	2.0	411	4.1	19	38.87r	0.073
NGC 5005	L1.9	SAB(rs)bc	4.0	948	21.3	103	39.47	0.650
NGC 5055	T2	SA(rs)bc	4.0	504	7.2	34	38.62r	0.170u
NGC 5377	L2	(R)SB(s)a	1.0	1792	31.0	150	39.18	0.250
NGC 5678	T2	SAB(rs)b	3.0	1924	35.6	172	39.19	0.079
NGC 5879	T2/L2	SA(rs)bc?	4.0	772	16.8	81	38.32	0.160
NGC 5921	T2	SB(r)bc	4.0	1479	25.2	122	39.15r	0.110
NGC 5970	L2/T2:	SB(r)c	5.0	1965	31.6	153	38.06	0.180c
NGC 5982	L2::	E3	-5.0	2904	38.7	187	38.46c	0.490u
NGC 5985	L2	SAB(r)b	3.0	2518	39.2	190	38.94	0.300
NGC 6340	L2	SA(s)0/a	0.0	1207	22.0	106	38.50	0.430b
NGC 6384	T2	SAB(r)bc	4.0	1667	26.6	128	38.12	0.150u
NGC 6482	T2/S2::	E:	-5.0	3921	52.3	253	39.23	0.130u
NGC 6500	L2	SAab:	1.7	2999	39.7	192	40.31	0.230
NGC 6501	L2::	SA0+:	-0.5	2869	39.6	191	38.01c	0.870u
NGC 6503	T2/S2:	SA(s)cd	6.0	42	6.1	29	37.56	0.080
NGC 6702	L2::	E:	-5.0	4712	62.8	304	38.61c	0.620u
NGC 6703	L2::	SA0-	-2.5	2364	35.9	174	38.51	0.360u
NGC 6951[3]	S2	SAB(rs)bc	4.0	1424	24.1	116	39.07	0.230
NGC 7177	T2	SAB(r)b	3.0	1147	18.2	88	38.94	0.140
NGC 7217	L2	(R)SA(r)ab	2.0	945	16.0	77	38.86	0.250
NGC 7331	T2	SA(s)b	3.0	821	14.3	69	38.49	0.097u
NGC 7626	L2::	E: pec	-5.0	3422	45.6	221	38.81	0.220u
NGC 7742	T2/L2	SA(r)b	3.0	1653	22.2	107	39.07	0.130
NGC 3367	H	SB(rs)c	5.0	3041	43.6	211	40.98	0.031
NGC 6217	H	(R)SB(rs)bc	4.0	1362	23.9	115	40.41	0.032
NGC 205	normal	dE5 pec	-5.0	-239	0.7	3	< 34.79r	...
NGC 221	normal	E2	-6.0	-205	0.7	3	< 36.16r	...
NGC 224	normal	SA(s)b	3.0	-298	0.7	3	...	...
NGC 628	normal	SA(s)c	5.0	655	9.7	3	< 36.69r	...
NGC 1023	normal	SB(rs)0-	-3.0	632	10.5	51	< 37.82r	...
NGC 2950	normal	(R)SB(r)0	-2.0	1337	23.3	204	< 38.42r	...
NGC 6654	normal	(R')SB(s)0/a	0.0	1823	29.5	123	< 38.11r	...

Note. — Col. (1): Galaxy name; Col. (2): Spectral class. Col. (3): Hubble type. Col. (4): Numerical Hubble type. Col. (5): Radial velocity. Col. (6): Distance. Col. (7): Angular scale. Col. (8): Hα luminosity. Col. (9): [OI]/Hα flux ratio. All quantities were extracted from HFS97. Revised values of log $L_{H\alpha}$, taken from Ho et al. (2003), are indicated by an "r" in column 8. See HFS97 for the meaning of other notes on columns 8 and 9.

[1,2]Grouped among TOs in this paper.

[3]Grouped with LINERs in this paper (see Pérez et al. 2000).

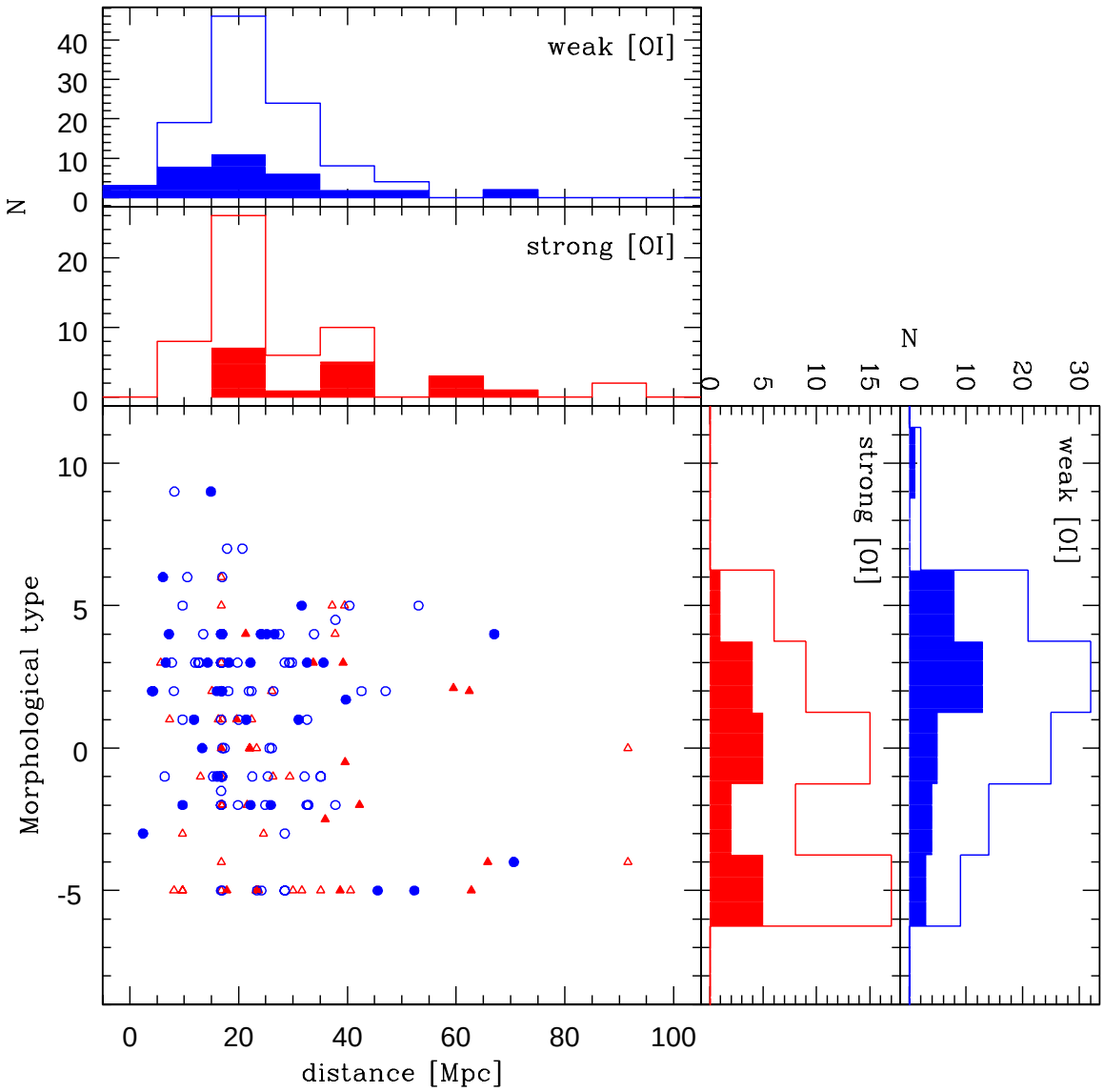

Fig. 1.— Distances and morphological T types for the strong-[OI] (triangles, [OI]/H$\alpha > 0.25$) and weak-[OI] LLAGN (circles, [OI]/H$\alpha \leq 0.25$) in the HFS sample. Filled symbols and filled areas in the histograms indicate objects in our sample. (All data extracted from HFS97.)

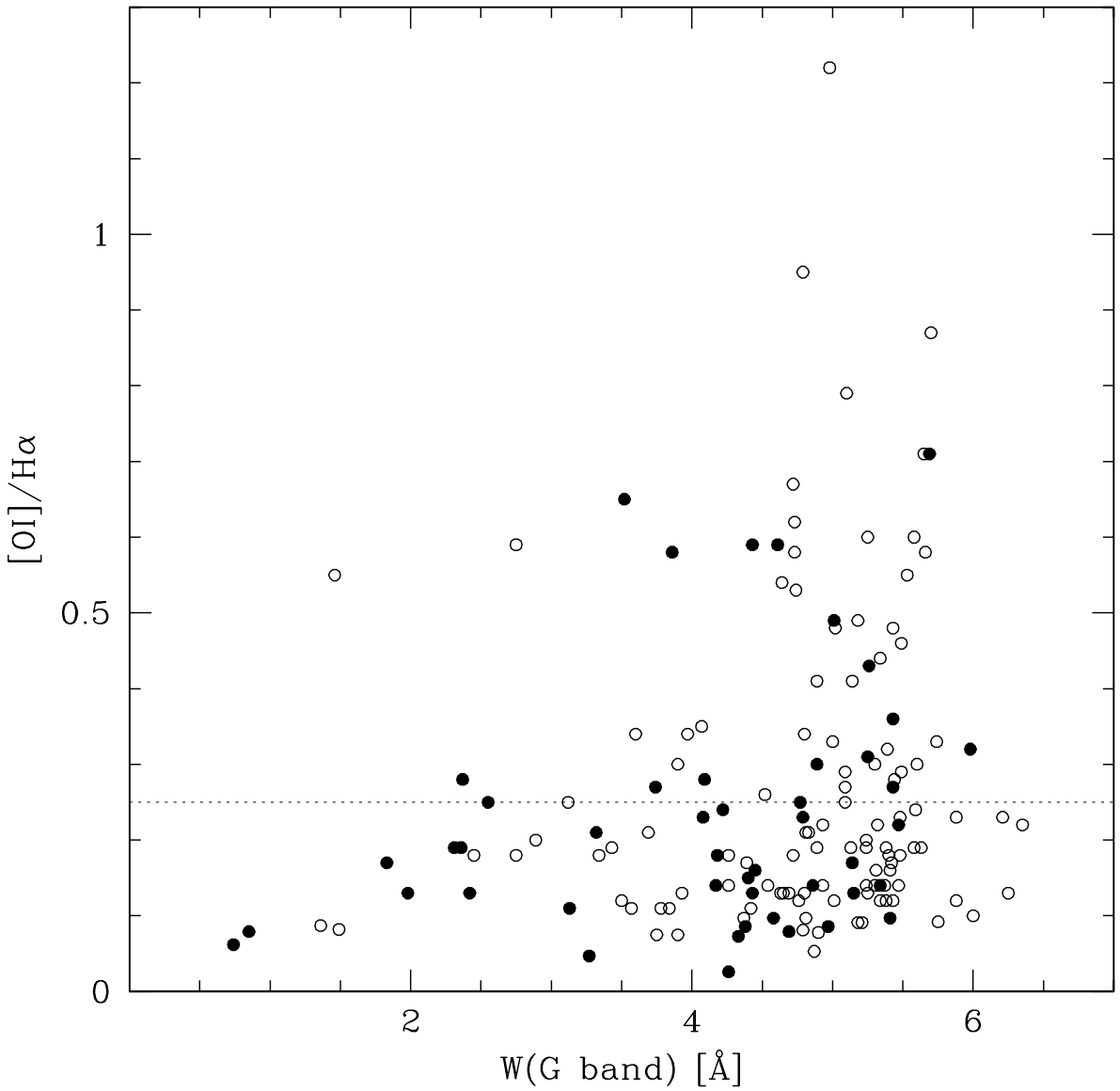

Fig. 2.— Equivalent width of the G band versus [OI]/Hα for LLAGN in the HFS sample. Filled symbols mark objects in our sample. The horizontal line at [OI]/H$\alpha = 0.25$ indicates our border-line between weak and strong-[OI] nuclei. (All data extracted from HFS97.)

symbols mark objects which we have observed. The visual impression from the bottom left plot is that our galaxies are well mixed within the HFS sample. This is confirmed by the histograms projected along both axis of Figure **??**, where we see that our galaxies (filled areas) follow reasonably well the distributions of d and T in the full HFS sample (solid lines). In both samples the distribution of morphological types of weak-[OI] nuclei is skewed towards somewhat later type hosts than for strong-[OI] nuclei, but with a substantial overlap, as discussed by Ho et al. (2003).

In Figure **??** we compare the G band equivalent width and the [OI]/Hα ratio, both extracted from HFS97. Again, one sees that our galaxies are well mixed within the HFS galaxies. This is confirmed by a statistical analysis. The mean value and rms dispersion of W(G band) is 4.6 ± 1.2 for all LLAGN in HFS97 and 4.1 ± 1.3 in our sample. No biases were detected in the [OI]/Hα ratio either (0.27 ± 0.21 compared to 0.25 ± 0.19 for the HFS and our samples respectively), and similar results apply to other stellar indices and emission line ratios tabulated by HFS97. We thus conclude that our sample is representative of the full HFS sample in terms of emission line and stellar population properties.

We note in passing that Figure **??** already gives away an important result of this investigation. Most objects with a weak G band are also weak [OI] emitters. The "inverted L" shape traced by the galaxies in this plot is only spoiled by a streak of 3 or 4 LINERs with [OI]/H$\alpha \sim 0.6$ and W(G band) < 4 Å. Apart from these objects, the top-left region of Figure **??** is remarkably empty. Of the two objects which intrude most in this "zone of avoidance", NGC 5195 and IC 239, the latter has only an upper limit on [OI] and both have uncertain classifications (HFS97). Similar uncertainties affect several other points in Figure **??**, but these do not affect the global shape of the distribution. Other versions of this plot are presented and discussed in §6.

3. Observations

Observations were carried out in four runs at the 2.5m Nordic Optical Telescope and one run at the Kitt Peak National Observatory 2.1m. The NOT observations used the ALFOSC detector with grism number 6 and a $1''$ wide slit, which gives a dispersion of 1.4 Å per pixel and covers the wavelength range 3500–5500 Å. The slit was oriented along the paralactic angle. Most observations were made under sub-arcsecond seeing and photometric conditions. The KPNO observations were carried out using the Gold Camera with grating 26 old and a slit $2''$ wide, which gives a dispersion of 1.24 Å per pixel, and covers the 3400–5500 Å interval. The slit was oriented in the N–S direction and the observations were done as close to the meridian passage as possible to avoid light losses by differential refraction. The weather

Table 2. Log of observations

Name	Telescope	Date	Exposure (s)	airmass
NGC 266	NOT	8-21-01	3x1200	1.03
NGC 315	NOT	8-22-01	3x1200	1.11
NGC 404	KPNO	7-26-01	2x1200	1.29
NGC 410	NOT	8-21-01	3x1200	1.13
NGC 428	NOT	8-23-01	4x1200	1.26
NGC 521	NOT	8-23-01	3x1200	1.69
NGC 660	NOT	8-21-01	4x1200	1.07
NGC 718	NOT	8-22-01	3x1200	1.20
NGC 772	NOT	8-23-01	3x1200	1.04
NGC 841	NOT	8-22-01	4x1200	1.02
NGC 1052	NOT	8-22-01	2x1200	1.26
NGC 1161	NOT	8-23-01	2x1200	1.06
NGC 1169	NOT	11-8-02	3x1200	1.05
NGC 2681	NOT	11-8-02	3x900	1.33
NGC 2685	NOT	11-8-02	3x1200	1.03
NGC 2911	NOT	5-3-03	3x1200	1.12
NGC 3166	NOT	5-4-03	2x1200	1.11
NGC 3169	NOT	5-3-03	3x1200	1.14
NGC 3226	NOT	5-14-01	3x1200	1.05
NGC 3245	NOT	5-12-01	1800+1200+600	1.04
NGC 3627	NOT	5-13-01	3x1200	1.09
NGC 3705	NOT	5-14-01	3x1200	1.12
NGC 4150	NOT	5-14-01	4x1200	1.28
NGC 4192	NOT	5-12-01	4x900	1.04
NGC 4438	NOT	5-15-01	4x1200	1.25
NGC 4736	NOT	5-3-03	3x900	1.04
NGC 4569	NOT	5-12-01	3x1200	1.11
NGC 4826	NOT	5-14-01	3x1200	1.26
NGC 5005	NOT	5-3-03	3x1200	1.09
NGC 5055	NOT	5-15-01	4x1200	1.15
NGC 5377	NOT	5-3-03	3x1200	1.24
NGC 5678	NOT	5-13-01	4x1200	1.18
NGC 5879	NOT	5-14-01	4x1200	1.21
NGC 5921	NOT	5-12-01	3x1200	1.09
NGC 5970	NOT	8-23-01	3x1200	1.19
NGC 5982	NOT	5-4-03	3x1200	1.28
NGC 5985	NOT	8-22-01	3x1200	1.29
NGC 6340	KPNO	7-26-01	3x1200	1.34
NGC 6384	NOT	5-13-01	3x1200	1.12
NGC 6482	NOT	5-12-01	3x1200	1.03
NGC 6500	NOT	5-12-01	3x1200+900	1.02
NGC 6501	NOT	8-22-01	3x1200	1.10
NGC 6503	NOT	5-13-01	3x1200	1.33
NGC 6702	NOT	8-21-01	3x1200	1.06
NGC 6703	KPNO	7-24-01	3x1200	1.03
NGC 6951	KPNO	7-24-01	2x1200	1.21
NGC 7177	KPNO	7-25-01	3x1200	1.20
NGC 7217	KPNO	7-26-01	3x1200	1.01
NGC 7331	KPNO	7-24-01	3x1200	1.03
NGC 7626	NOT	8-23-01	3x1200	1.40
NGC 7742	KPNO	7-24-01	2x1200	1.10
NGC 3367	NOT	5-13-01	3x1200	1.04
NGC 6217	NOT	8-23-01	3x1200	1.62
NGC 205	NOT	11-7-02	3x900	1.03
NGC 221	NOT	11-7-02	2x1200	1.22
NGC 224	NOT	11-7-02	2x900+600	1.08
NGC 628	NOT	11-7-02	3x1200	1.03
NGC 1023	NOT	11-7-02	3x900	1.10
NGC 2950	NOT	11-7-02	3x900	1.21
NGC 6654	NOT	5-15-01	3x1200	1.41

during the observations was not photometric, and the seeing was typically 2–3″. A log of the observations is given in Table **??**.

The data were reduced using standard IRAF procedures. The individual frames were overscanned, bias subtracted and flat field divided. The calibration also followed standard steps. The wavelength scale was calibrated using an HeNeAr lamp. The flux calibration was done with observations of spectrophotometric standard stars observed with a slit width of 10″. The individual frames were combined using crreject task in IRAF to remove cosmic rays. Sky was subtracted with the background task fitting a polynomium along the spatial light profile.

3.1. Nuclear Extractions

Most of the spectra have excellent signal out to several arcsec from the nucleus. In Cid Fernandes et al. (2003b, Paper III) we explore this spatial information to map the stellar populations in the central regions of these objects, in analogy with previous work for type 2 Seyferts (Cid Fernandes, Storchi-Bergmann & Schmitt 1998; Joguet et al. 2001; Raimann et al. 2003). In this paper we concentrate on the nuclear spectra. Off-nuclear extractions will only be used as templates for the nuclear spectra (§**??**).

Nuclear spectra were extracted from the central 1″×1.1″ (6 pixels) for the 52 galaxies observed at NOT and 2″×2.3″ (3 pixels) for the 8 galaxies observed at KPNO. Using the distances in Table **??**, the projected areas covered by these extractions correspond to radii of 11–204 pc, with a median value of 71 pc considering only the LLAGN in the sample. The signal-to-noise ratio was estimated from the rms fluctuation in the 4789–4839 Å interval, which is free of major absorption or emission features. We obtain S/N in the 23–88 range, with a median value of 50. In the 4010–4060 Å interval the median S/N is 22.

3.2. HFS extractions

Most of the HFS97 spectra were collected through a $2'' \times 4''$ aperture, ~ 7 times larger in area than our typical nuclear extractions. In order to allow a more meaningful comparison of our measurements with those in HFS97 we have also extracted spectra through a $2'' \times 4''$ aperture (hereafter the "HFS-aperture"). This was straightforward for the KPNO observations, which have a slit width equal to that in HFS97. In order to construct an HFS-aperture for the NOT data, which was collected through a 1″ slit, we first extracted a 4″ long spectrum and then multiplied it by 2 except in the nucleus (ie, the inner 1.1″),

which was represented by an interpolation between off-nuclear extractions centered at $\pm 1.1''$ to avoid overweighting any nuclear point source. The flux in this approximate HFS-aperture is typically 4 times larger than in our nuclear extractions.

All spectral properties discussed in §**??** were measured both through our nuclear extractions and through this HFS-aperture, but only the nuclear values are published here, since except for galaxies with noticeable gradients (discussed in Paper III) the results are similar for both apertures. Tables for HFS-apertures measurements are available upon request.

Besides spatial resolution, our observations differ from those of HFS97 in spectral coverage. The blue spectra in HFS97 cover the 4230–5110 Å interval, while our spectra go from 3500 up to 5500 Å. As well shall soon see, the region between 3500 and 4200 Å proved to be most revealing.

4. Spectra

In this section we present the spectra and two different methods to characterize the stellar populations in the central regions of LLAGN. The first method consists of an empirical, qualitative classification based on the comparison with non-active galaxies representative of simple stellar populations with different ages. The second method quantifies this classification by modeling the starlight using the non-active galaxies as spectral templates. In Section 5 we present measurements of several spectral indices (such as the 4000 Å break, Hδ, CaII K, G band and others), which provide yet another way to characterize stellar populations. A comparison of all these methods is important in view of the diversity of methods to analyse the stellar populations of AGN found in the literature. This comparison allows us to do a relative calibration between them, and can be used to convert the results obtained with one method to the others.

4.1. Normal galaxies and an empirical stellar population classification

We start our presentation of the nuclear spectra by the 9 non-active galaxies in our sample, shown in Figure **??**. The order of the spectra in this plot reflects approximately the age of the dominant stellar population, younger systems at the top. These normal galaxy spectra are used in this work as a reference basis for an empirical stellar population classification. Galaxies in Figure **??** can be separated into four classes:

(Y) Galaxies with evidently young, $< 10^7$ yr, stellar populations (NGC 3367 and NGC

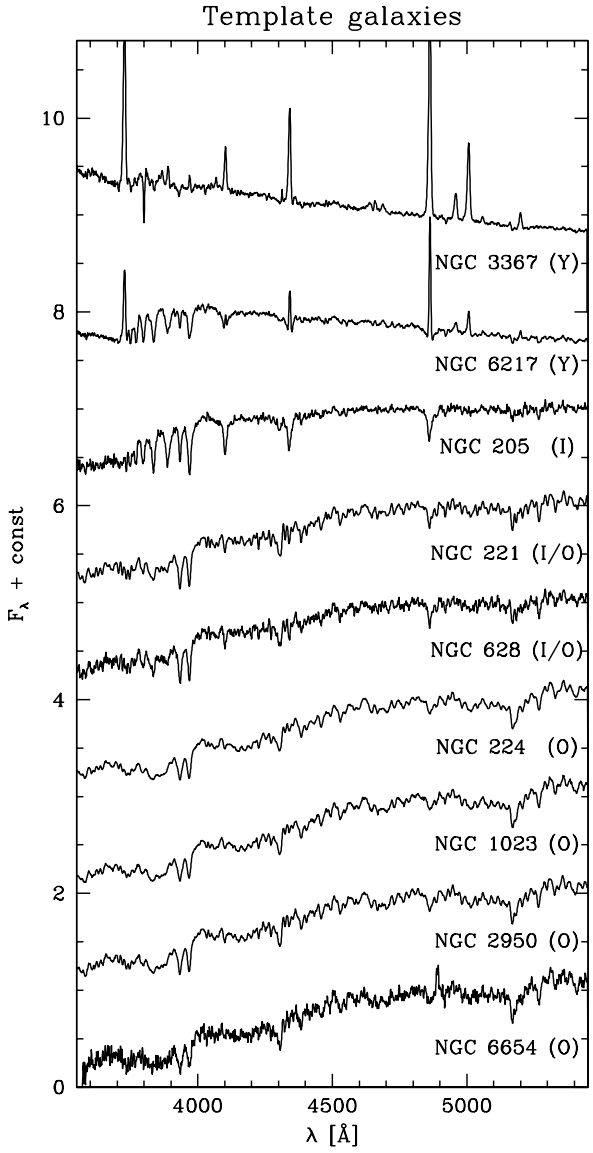

Fig. 3.— Spectra of the normal galaxies in the sample, including two Starburst nuclei (top). Galaxies are sorted according to the age of the dominant stellar population, with younger systems at the top. Y, I, I/O and O denote our empirical stellar population classes.

6217), characterized by a blue continuum and weak metal absorption lines;

(I) galaxies with a dominant intermediate age, 10^8–10^9 yr population, characterized by pronounced HOBLs (NGC 205);

(I/O) galaxies with a mixture of intermediate age and older stars (NGC 221 and NGC 628);

(O) galaxies dominated by an old stellar population (NGC 224, NGC 1023, NGC 2950 and NGC 6654), characterized by strong metal lines.

For short, these four stellar population classes are denominated Y, I, I/O and O, respectively. We use the symbol η to denote these classes.

We have compared each of the LLAGN in our sample to these normal galaxies and classified them onto these same 4 stellar population categories according to a similarity criterion. This was first done by a simple visual inspection of the spectra, and later confirmed by means of the starlight modeling scheme described in §**??**. The results are listed in the last column of Table **??**. None of the objects resembles predominantly young systems like NGC 3367, so all our LLAGN fall onto the $\eta = I$, I/O and O categories.

This empirical classification provides a stellar population counterpart to the LINER/TO classification, which is based on emission line properties. The η classes are used here just as a heuristic aid to sort the LLAGN spectra according to their main stellar populations. This is a useful strategy to investigate connections between emission line and stellar population properties. However, classification criteria, while certainly helpful to identify general trends, have a certain degree of uncertainty and arbitrariety. When discussing our results we will thus not restrict ourselves to comparisons between discrete emission line and stellar population classes. In §**??** we give more emphasis to comparisons between continuous stellar population and emission line properties. We shall see that a clearer picture emerges if one avoids the rigidity of taxonomy.

4.2. LINERs and Transition Objects

The nuclear spectra for all LLAGN in our sample are shown in Figures **??**–**??**. Since our main aim in this paper in to investigate the relation between the stellar populations of these objects and their emission line properties, we have split the spectra in six slots: strong-[OI] sources with either O, I/O and I stellar population characteristics (Figures **??** and **??**) and weak-[OI] with either $\eta = O$, I/O and I (Figures **??**, **??** and **??**).

As is typical of LLAGN, the spectra are completely dominated by starlight. With few exceptions (eg, NGC 1052 and NGC 6501), emission lines are generally weak, and sometimes altogether absent (eg, NGC 410 and NGC 5055). Important diagnostic lines like Hβ and [OIII]$\lambda\lambda$4959,5007 are rarely seen, although [OII]λ3727 is detected in most spectra. As thoroughly discussed and illustrated by HFS97, starlight subtraction is an absolute necessity in order to measure emission lines in these objects, so we postpone the analysis of emission lines to a future communication. Except for [OII], lines fluxes for galaxies in the present sample have already been measured by HFS97, including the important region around Hα, so we will use their measurements when necessary. In the following we concentrate on the measurement and analysis of stellar population features.

As is evident from Figures **??**–**??**, there is a clear connection between stellar population characteristics and the emission line properties encoded in the weak/strong-[OI] classification. Old stellar populations are substantially more frequent in strong than in weak-[OI] sources, whereas the opposite happens for stellar population class I. Numerically, we find that out of our 17 strong-[OI] nuclei, 10 (59%) are in the $\eta = O$ class, 5 (29%) have $\eta = I/O$ and only 2 (12%) belong to the $\eta = I$ class, while the corresponding numbers for the 34 weak-[OI]'s are 7 (21%), 11 (32%) and 16 (47%) respectively.

4.3. High Order Balmer Absorption Lines

The most notable feature in this data set is the ubiquity of the HI high order Balmer series in absorption (H8 and higher), particularly among weak-[OI] nuclei. By definition, objects where these features are clearly present are attributed $\eta = I$ (ie, they resemble NGC 205). Systems with HOBLs are also bluer and have shallower metal absorption lines than the rest. Overall, their spectra reveal clear signs of a 10^8–10^9 yr intermediate age, "post-starburst" population. HOBLs may also be present in I/O nuclei, but blended with metal lines of old stars to such an extent that they do not stand out clearly in the total spectrum.

HOBLs have been seen before in a few LLAGN, the most famous example being NGC 4569 (Keel 1996), which is also in our sample (Figure **??**a). However, an incidence rate as high as that suggested by our survey had not been suspected before. Ho et al. (2003) argue that objects like NGC 4569 are not representative of LLAGN in their sample, most of which have a "demonstrably old" stellar population. While we agree that NGC 4569 is an extreme example and that old stars dominate the light in most LLAGN, our spectra reveal the presence of intermediate age stars in at least 1/3 of the objects. The reason why we identify more of these populations than Ho et al. (2003) is that they had to base their judgment on the strength of the Hγ, Hβ and Hα absorptions, which are much more affected

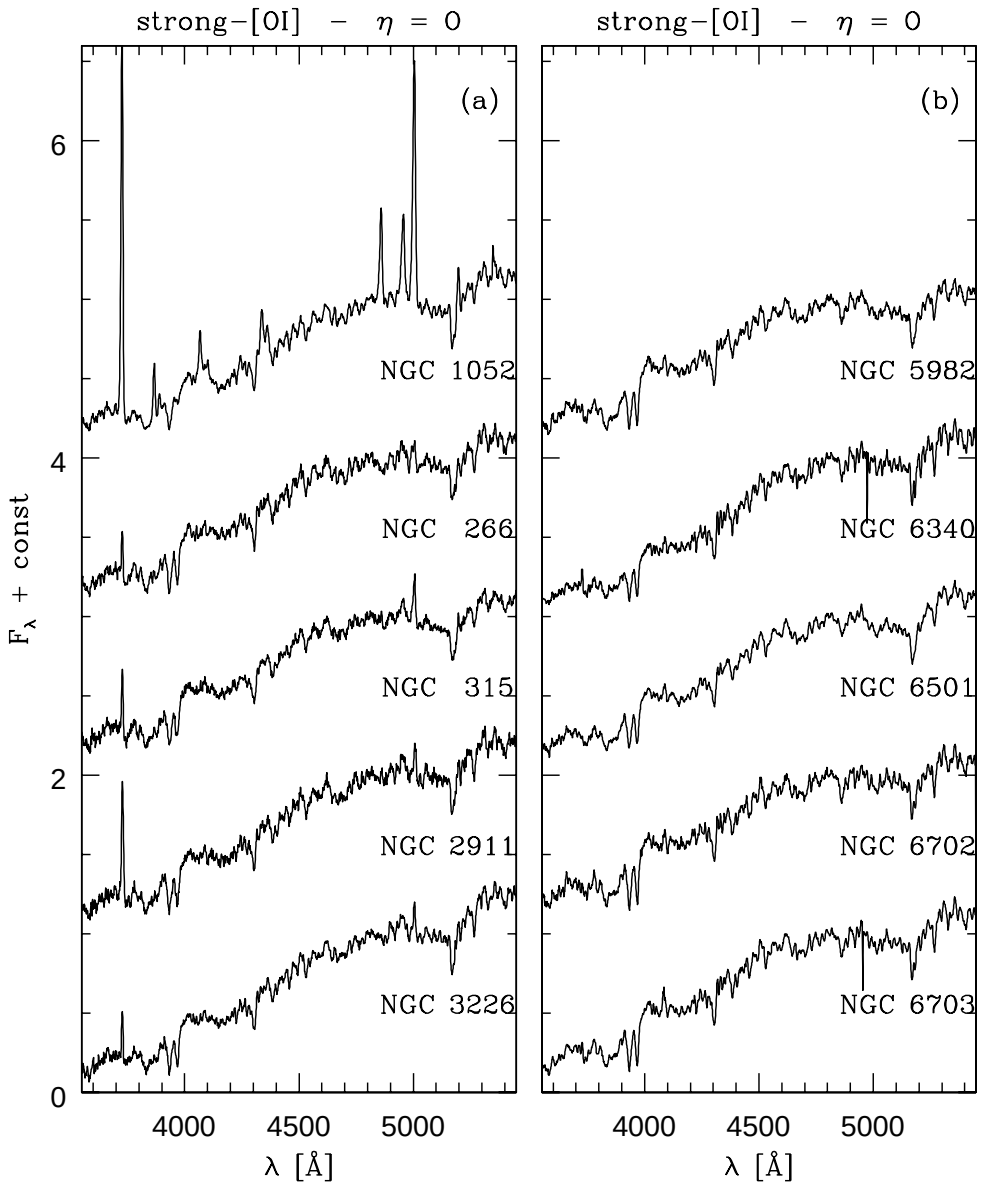

Fig. 4.— Nuclear spectra of strong-[OI] LLAGN with predominantly old stellar populations ($\eta = O$).

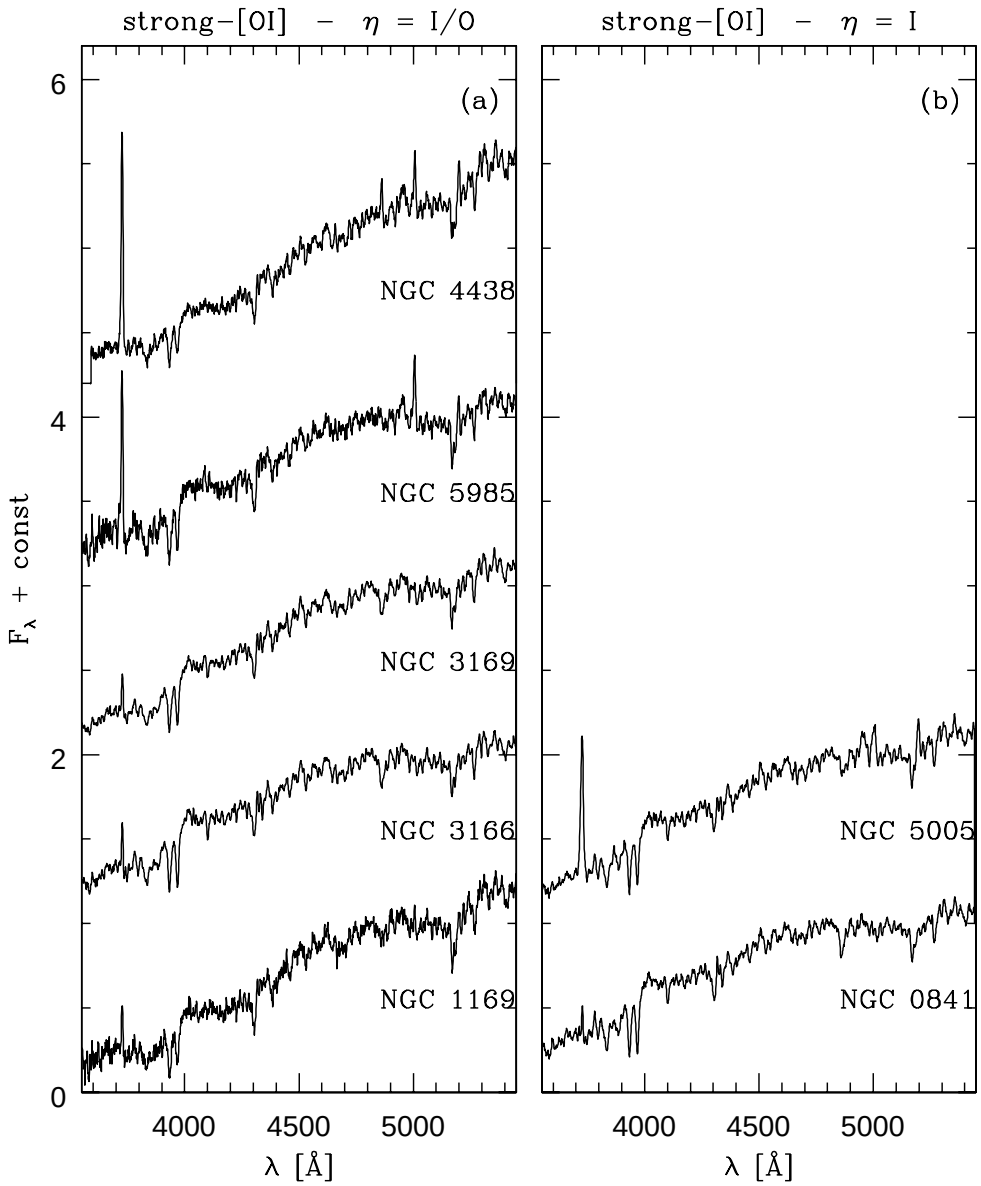

Fig. 5.— Nuclear spectra of strong-[OI] LLAGN with stellar population classes $\eta = I/O$ (a) and $\eta = I$ (b).

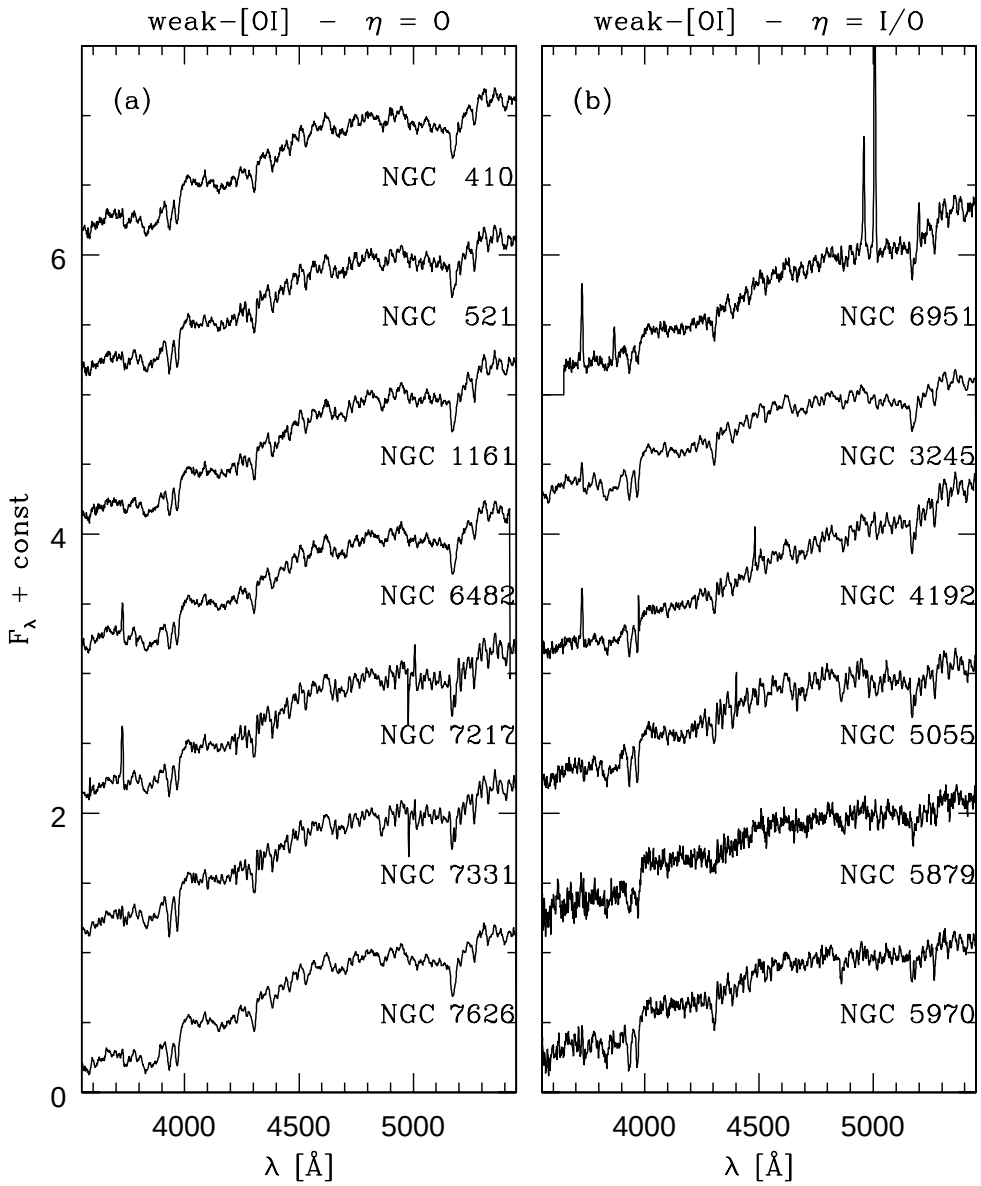

Fig. 6.— Nuclear spectra of weak-[OI] LLAGN with stellar population classes $\eta = O$ (a) and $\eta = I/O$ (b).

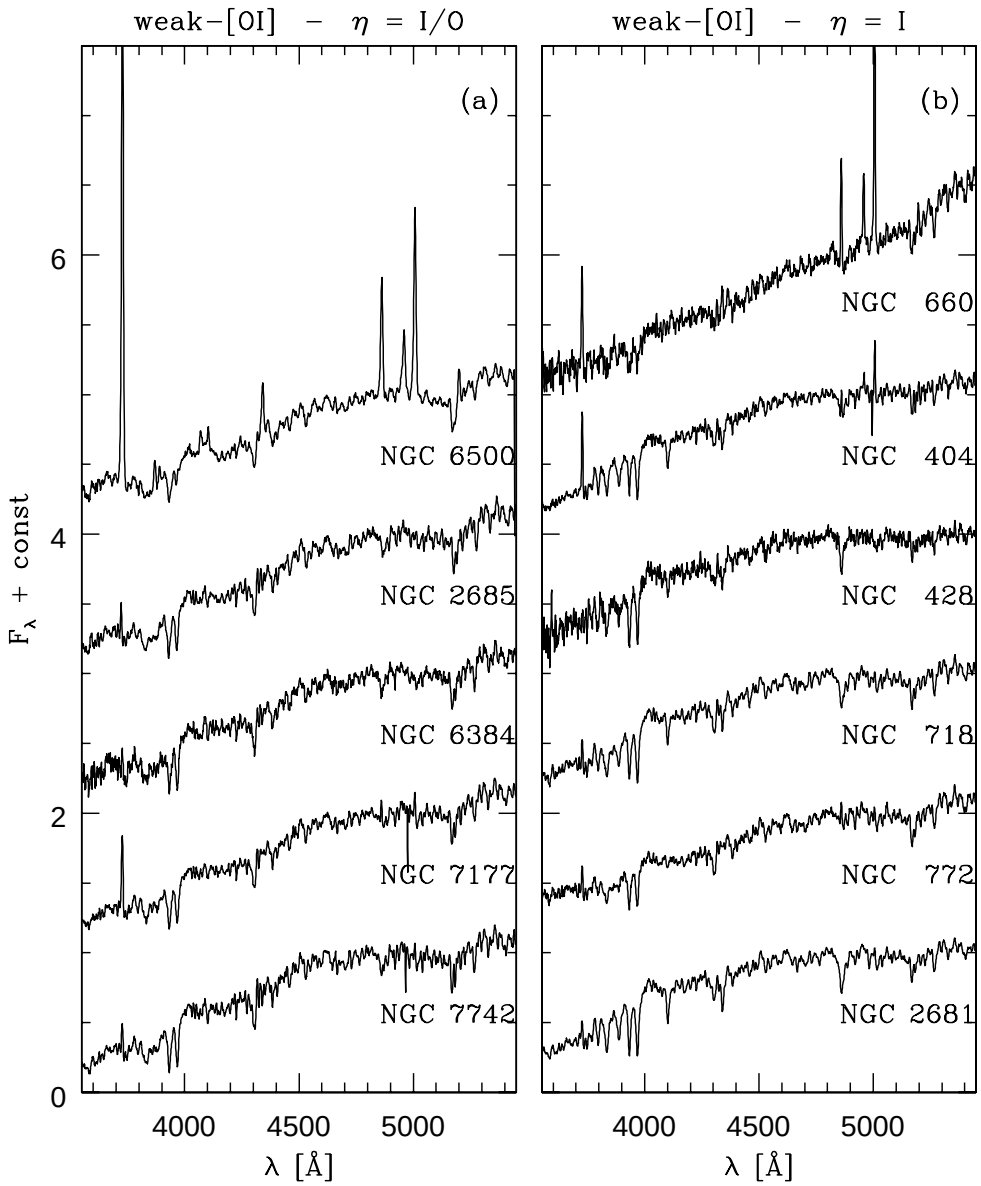

Fig. 7.— Nuclear spectra of weak-[OI] LLAGN with stellar population class $\eta = I/O$ (a) and $\eta = I$ (b).

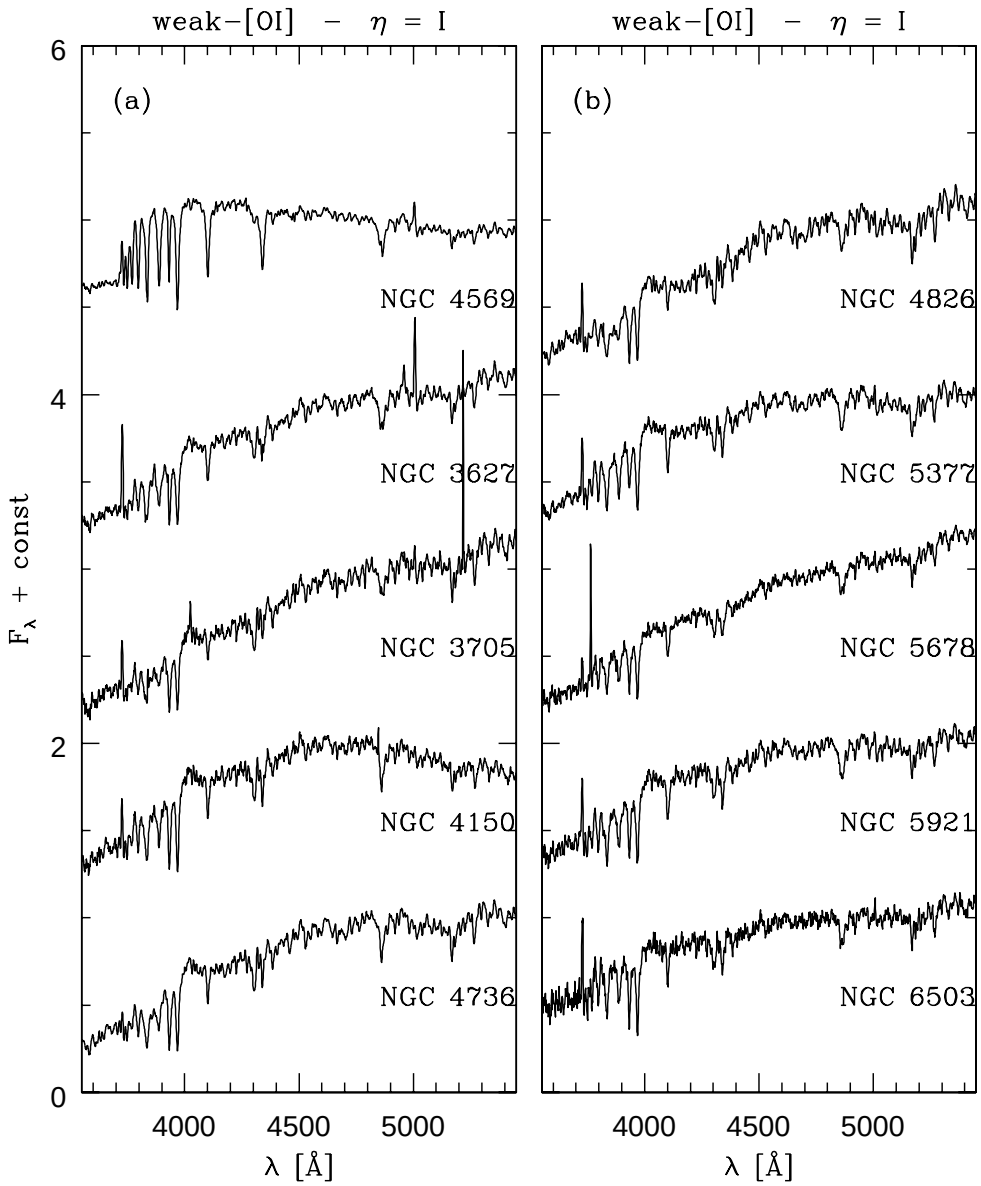

Fig. 8.— Nuclear spectra of weak-[OI] LLAGN with a strong intermediate age stellar population ($\eta = I$).

by emission and dilution by old stars than HOBLs.

As remarkable as the high frequency of HOBLs in weak-[OI]'s is their apparent dearth among strong-[OI] nuclei. HOBLs are ~ 5 times more frequent in weak than in strong-[OI] sources ($\eta = I$ fractions of $\sim 50\%$ compared to $\sim 10\%$ respectively). These findings reveal a strong link between the central stellar populations and emission line properties, particularly [OI]/Hα.

The statistics above obviously depend on our adopted borderline between weak and strong-[OI] nuclei (at [OI]/H$\alpha = 0.25$), but the dichotomy persists (albeit somewhat diluted) even if one adopts the HFS97 [OI]/H$\alpha = 0.17$ classification criterion. A less classification dependent assessment of the relation between stellar and emission line properties is presented in §**??**, where we replace the discrete stellar population and emission line classes used above by a more continuous description.

4.4. Empirical starlight modeling

As noted in §1, the location of TOs in between LINERs and HII-nuclei in diagnostic diagrams suggests that their emission line spectrum results from a mixture of AGN spectrum plus photoionization by young stars (HFS97). If this is the case, one would expect to find direct signatures of stellar populations of 10^7 yr or less in their spectra. Although the high incidence rate of HOBLs among weak-[OI] nuclei points to some sort of connection between stellar populations and emission line properties, these features signal the presence of a $\sim 10^8$–10^9 yr post-starburst-like component, not a young starburst. The clearest single signature of young stars in the spectral range covered by our data is the WR bump at 4680 Å. This feature is not evident in any of our LLAGN spectra. The WR bump was only detected in the Starburst galaxy NGC 3367 (Figure **??**), which is part of our comparison sample.

Given the dominance of old and intermediate age stars in LLAGN, a weak young starburst (with or without a correspondingly weak WR bump) could well be lurking in some of our spectra. Detailed modeling of the stellar population mixture is required to evaluate this possibility. This modeling is performed in a separate communication (Paper II), in order not to mix data with models. In this paper we want to keep the analysis at a more empirical level. We have thus implemented an entirely self contained starlight modeling technique which, instead of resorting to theoretical spectra, uses only our observed spectra.

Each spectrum was modeled as a combination of a base of template spectra. Two bases were considered: A "normal galaxy base", containing five spectra from our comparison sample (NGC 3367, NGC 205, NGC 221, NGC 1023 and NGC 2950), and an "off-nuclear

base", containing two off-nuclear extractions centered at $\pm 2.4''$ from the nucleus. Except for the possibility of using off-nuclear templates, this procedure is very similar to the one employed by HFS97 in their starlight subtraction scheme.

All spectra were normalized to the flux at 4020 Å and corrected for Galactic extinction prior to the modeling. The A_B values of Schlegel, Finkbeiner Davis (1998), extracted from NED[5], and the reddening law of Cardelli, Clayton & Mathis (1989) were used for this purpose. Intrinsic extinction by an uniform screen of dust was allowed for. An algorithm was developed which searches for the combination of base spectra and extinction which best reproduces the nuclear spectrum of each LLAGN. The code was adapted from the empirical population synthesis code of Cid Fernandes et al. (2001b) by simply replacing its spectral base by the full spectra in either one of these two bases. Regions around emission lines were masked out in the comparison between observed and model spectra. For the off-nuclear base, in most cases it was sufficient to mask out regions of 50 Å around [OII], Hβ and [OIII]. For the normal galaxy base we further masked regions around Hγ, Hδ and [NI]λ5200 since these are rather strong in the spectrum of NGC 3367, included in this base to represent a young starburst.

The presence of an emission line object in the normal galaxy base is another difference with respect to the starlight modeling scheme employed by HFS97. This difference is easily understood. HFS97 were interested in measuring emission lines from a starlight free spectrum, so their starlight templates were constructed out of galaxies without emission lines. Our interest here is quite the opposite: We want to analyze the starlight itself, not the emission lines. NGC 3367 was introduced in the fitting to evaluate how strong a young starburst can be accommodated in our LLAGN spectra. A consequence of this choice is that our observed minus model residual spectra will have underestimated, emission line fluxes when the NGC 3367 component is present in a significant proportion. There is no way of circumventing this without editing out the emission lines from NGC 3367 or resorting to theoretical stellar population spectra, since an emission line free starburst does not exist in nature. Nevertheless, in the majority of cases we find that the NGC 3367 component contributes very little ($\leq 2\%$) to the optical flux. In these cases, our residual spectra can be seen as pure emission spectra.

Examples of the results obtained with both spectral bases are shown in Figure **??**. The top panels show the observed spectrum ($F_\lambda^{\rm obs}$, thick line) and the two models for the starlight spectrum. The middle spectrum shows $F_\lambda^{\rm temp}$, the template constructed out of

[5]The NASA/IPAC Extragalactic Database (NED) is operated by the Jet Propulsion Laboratory, California Institute of Technology, under contract with the National Aeronautics and Space Administration.

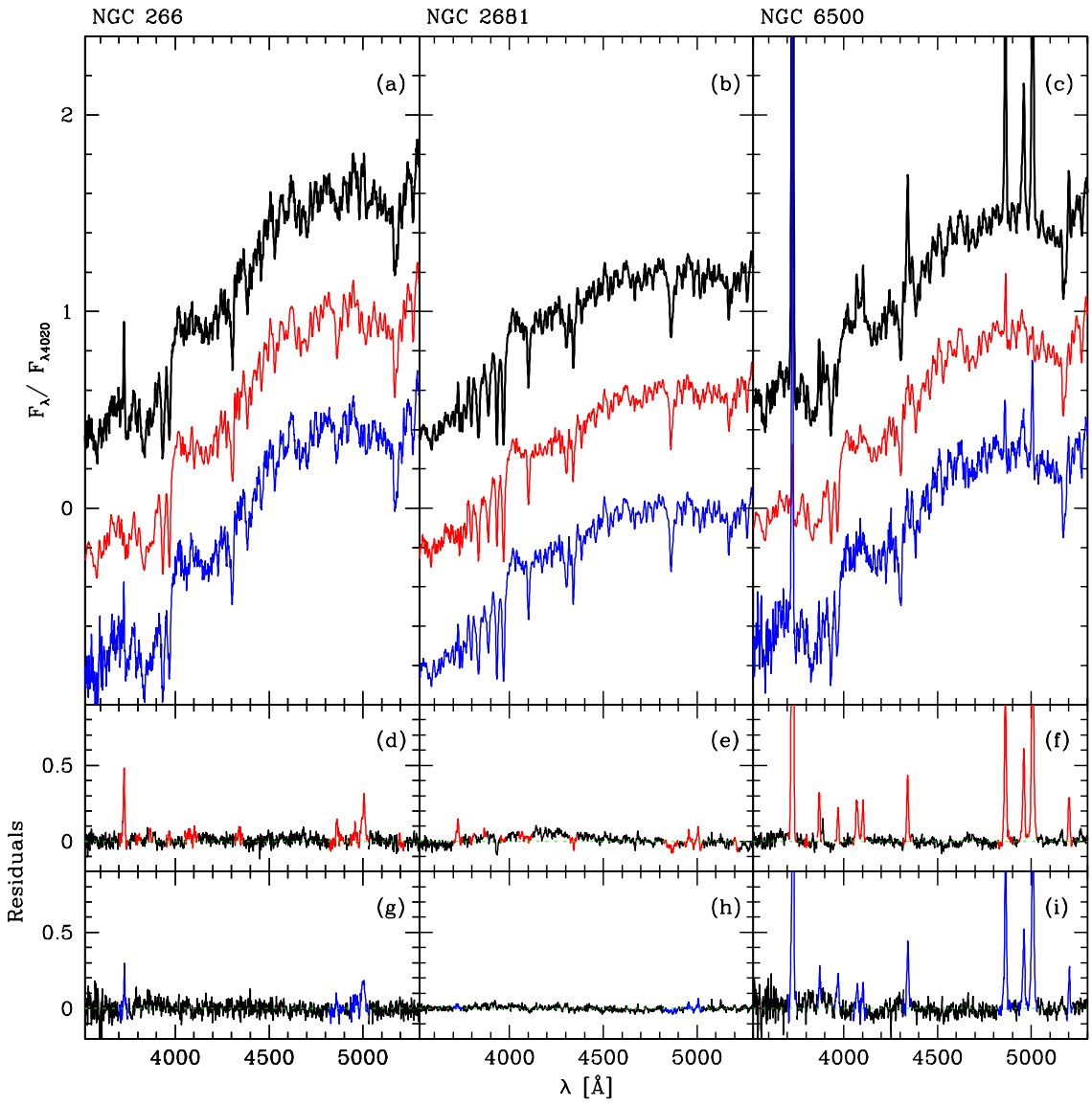

Fig. 9.— Results of the starlight modeling for NGC 266 ($\eta = O$, strong-[OI]), NGC 2681 ($\eta = I$, weak[OI]) and NGC 6500 ($\eta = I/O$, weak-[OI]). *(a–c):* The top panels show the nuclear spectrum F_λ^{obs} (top) and two starlight models: $F_\lambda^{\rm temp}$ (middle), constructed out of linear combinations of the normal galaxies NGC 3367, NGC 205, NGC 221, NGC 2950 and NGC 1023; and $F_\lambda^{\rm off-nuc}$ (bottom), constructed combining two off-nuclear extractions. All spectra are normalized to the flux at 4020 Å, and the two models are shifted downwards for clarity. *(d–f):* $F_\lambda^{\rm obs} - F_\lambda^{\rm temp}$ residual spectra. *(g–i):* $F_\lambda^{\rm obs} - F_\lambda^{\rm off-nuc}$.

linear combinations of the normal galaxy base, while the bottom spectrum ($F_\lambda^{\rm off-nuc}$) is the combination of two off-nuclear extractions which best matches the nuclear spectrum. Both models were shifted vertically for clarity. The residual spectra are shown in the bottom plots. Panels d–f correspond to $F_\lambda^{\rm obs} - F_\lambda^{\rm temp}$, while panels g–i show $F_\lambda^{\rm obs} - F_\lambda^{\rm off-nuc}$. Except for regions containing emission lines, the typical difference between $F_\lambda^{\rm obs}$ and the $F_\lambda^{\rm temp}$ model is better than 3% for all cases shown. This is comparable to the noise level. Off-nuclear templates produce equally good results for the examples shown, with residuals of 4% for NGC 266 and NGC 6500 and 1% for NGC 2681. In some cases (eg, NGC 772, NGC 4569, NGC 5921) the $F_\lambda^{\rm obs} - F_\lambda^{\rm off-nuc}$ residual reveals a nuclear blue component not present in the off-nuclear spectra. This happens specially in objects which have strong young and/or intermediate age populations as revealed by the strength of the NGC 3367 and NGC 205 components in the normal galaxy decomposition. We also note in passing that Figure **??** shows that HOBLs are present not only in the nucleus of NGC 2681, but also in off-nuclear extractions. The region producing the HOBLs is therefore *spatially extended*, a result which is examined in more detail in Paper III.

One thus sees that, except for galaxies with noticeable gradients, both methods yield comparable accuracy. For our current purposes, the normal galaxy base is more relevant, since it provides a way of quantifying the stellar population mix in LLAGN. In fact, this decomposition method provides a quantitative basis for the comparative stellar population classification outlined in §**??**. To illustrate how this works, one can write the relative contributions at $\lambda = 4020$ Å of NGC 3367 ($\eta = Y$), NGC 205 ($\eta = I$), NGC 221 ($\eta = I/O$) and NGC 2950 plus NGC 1023 ($\eta = O$) as a normalized four-component vector $\mathbf{x} = (x_Y, x_I, x_{I/O}, x_O)$. For the $\eta = O$ nuclei of NGC 266 and NGC 7626 we find $\mathbf{x} = (0, 5, 18, 77)\%$ and $(1, 2, 0, 97)\%$ respectively, while for NGC 4438, which we classified as $\eta = I/O$, this vector is $(0, 3, 51, 46)\%$, and for the $\eta = I$ nucleus of NGC 5921 we find $(2, 70, 4, 24)\%$. In over 90% of the cases this scheme yields the same classification as that initially inferred by visual inspection of the spectra. In the few cases where a disagreement occurred, we adopted the visually estimated η class, although this has no consequence for the results of this paper.

The results of the starlight modeling in terms of the normal galaxy base are summarized in Table **??**. A first important result of this analysis is that 23 of our 51 LLAGN contain a NGC 205 component stronger than 20%. Except for NGC 5879, which has a noisy spectrum, all nuclei where $x_I > 30\%$ were classified as $\eta = I$ because of their conspicuous HOBLs. Between $x_I = 10\%$ and 30% some objects were classified as $\eta = I$ (NGC 772) and others as I/O (eg, NGC 4192, NGC 5055). The starlight analysis therefore confirms the high incidence rate of HOBLs in LLAGN, specially weak-[OI]'s, and helps quantifying the presence of these intermediate age populations in cases where their contribution to the optical spectrum is not visually obvious.

Table 3. Starlight modeling results

Galaxy	x_Y (NGC 3367)	x_I (NGC 205)	$x_{I/O}$ (NGC 221)	x_O (NGC 1023 + NGC 2950)	A_V	Δ	η
NGC 0266	0.1	5.2	17.8	77.0	0.18	2.8	O
NGC 0315	3.8	9.2	1.5	85.5	0.09	3.5	O
NGC 0404	0.0	78.5	0.0	21.5	0.90	6.6	I
NGC 0410	0.0	1.8	0.7	97.5	0.04	2.6	O
NGC 0428	0.0	49.8	0.0	50.2	0.31	8.7	I
NGC 0521	1.3	11.1	0.1	87.6	0.31	2.7	O
NGC 0660	0.0	59.4	0.0	40.6	2.38	11.7	I
NGC 0718	0.0	51.3	2.3	46.4	0.13	2.7	I
NGC 0772	32.1	10.9	24.4	32.5	0.38	1.8	I
NGC 0841	0.0	37.7	17.4	44.9	0.18	2.3	I
NGC 1052	16.5	0.0	0.5	83.0	0.57	3.0	O
NGC 1161	0.0	6.7	0.1	93.2	0.13	2.7	O
NGC 1169	0.0	0.0	48.2	51.8	0.26	5.7	I/O
NGC 2681	0.0	66.2	1.4	32.4	0.22	3.4	I
NGC 2685	0.3	0.9	50.5	48.4	0.21	4.9	I/O
NGC 2911	0.0	3.4	0.0	96.6	0.83	4.6	O
NGC 3166	0.0	28.8	9.4	61.8	0.19	2.3	I/O
NGC 3169	0.0	21.1	0.0	78.9	0.73	4.4	I/O
NGC 3226	0.0	2.7	0.0	97.3	1.08	4.2	O
NGC 3245	14.4	3.8	25.5	56.3	0.17	1.5	I/O
NGC 3627	0.0	66.6	1.4	32.0	0.47	3.0	I
NGC 3705	0.0	39.3	13.8	46.9	0.54	3.6	I
NGC 4150	0.0	66.8	32.0	1.2	0.00	6.5	I
NGC 4192	0.0	19.1	34.7	46.1	1.41	3.4	I/O
NGC 4438	0.0	2.6	50.9	46.5	1.48	2.9	I/O
NGC 4569	28.2	71.8	0.0	0.0	0.00	5.3	I
NGC 4736	0.0	48.8	0.0	51.2	0.07	2.3	I
NGC 4826	0.0	32.8	10.7	56.5	0.24	2.3	I
NGC 5005	0.0	45.1	0.4	54.5	0.77	3.7	I
NGC 5055	2.0	20.8	9.1	68.1	0.24	3.4	I/O
NGC 5377	0.0	76.8	0.1	23.1	0.02	2.5	I
NGC 5678	0.0	89.7	0.3	9.9	1.22	3.8	I
NGC 5879	0.0	52.0	0.9	47.1	0.46	7.3	I/O
NGC 5921	1.7	70.1	3.7	24.5	0.00	2.8	I
NGC 5970	0.0	5.7	56.4	37.9	0.13	4.6	I/O
NGC 5982	0.2	10.3	2.5	87.0	0.02	1.9	O
NGC 5985	0.0	6.8	34.4	58.8	0.19	4.9	O
NGC 6340	0.0	4.1	0.0	95.9	0.98	6.6	O
NGC 6384	1.2	2.2	61.3	35.3	0.02	4.4	I/O
NGC 6482	10.1	0.2	0.0	89.7	0.12	2.5	O
NGC 6500	24.7	0.1	4.0	71.3	0.08	2.3	I/O
NGC 6501	1.2	11.5	0.0	87.3	0.25	2.3	O
NGC 6503	22.5	55.8	16.3	5.4	0.32	3.0	I
NGC 6702	0.0	7.0	18.6	74.4	0.00	2.7	O
NGC 6703	0.0	3.4	0.0	96.6	0.22	3.5	O
NGC 6951	2.0	29.4	18.9	49.7	0.41	3.1	I/O
NGC 7177	2.4	13.7	43.1	40.8	0.39	2.8	I/O
NGC 7217	0.0	7.2	0.0	92.8	0.43	3.6	O
NGC 7331	0.0	5.3	15.0	79.8	0.37	2.8	O
NGC 7626	1.1	1.8	0.0	97.2	0.09	2.2	O
NGC 7742	0.0	14.3	0.0	85.7	0.16	4.1	I/O

Note. — Results of the starlight decomposition in terms of the normal galaxies NGC 3367, NGC 205, NGC 221, NGC 1023 and NGC 2950. Cols. (2)–(5): x_Y, x_I, $x_{I/O}$ and x_O, given as percentage fractions of the flux at 4020 Å. Col. (6): V band extinction (in mag) of the best fit. Col. (7): Mean absolute percentage difference between the observed and model spectra: $\Delta =< |F_\lambda^{\rm obs} - F_\lambda^{\rm model}|/F_\lambda^{\rm obs} >$. Col. (8): Stellar population class.

4.5. The weakness of young stellar populations in LLAGN

A second result of the starlight modeling is that few LLAGN have an optically relevant young starburst. The contribution of the NGC 3367 component is larger than 20% in just four cases. In order of decreasing x_Y, these are NGC 772 (32%), NGC 4569 (29%), NGC 6500 (25%) and NGC 6503 (22%), which are all weak-[OI]'s.

Of all our LLAGN, only NGC 6500 presents marginal evidence for the presence of the WR bump. This can be seen by the coherent broad residual with amplitude of no more than a few % in the $F_\lambda^{\rm obs} - F_\lambda^{\rm temp}$ residual spectrum in Figure **??**f. Naturally, the amplitude of this residual increases a bit removing the WR bump from the NGC 3367 base component, but even then we cannot claim a conclusive detection of this feature. One way to double check this possibility is to evaluate the residual spectrum obtained with the off-nuclear base. If WR stars are concentrated in the nucleus, a WR bump should appear in the $F_\lambda^{\rm obs} - F_\lambda^{\rm off-nuc}$ difference spectrum. In the case of NGC 6500, this residual reveals a weak narrow nebular HeIIλ4686, but no clear sign of a broad bump (Figure **??**i). A tentative detection of broad HeII in this galaxy has been previously reported by Barth et al. (1997).

Detecting the WR bump is already hard in *bona fide* Starburst galaxies (eg, Schaerer, Contini & Kunth 1999), and the superposition of a dominant older stellar population only makes matters worse. In NGC 3367 this feature has an equivalent width of ~ 5 Å, similar to the values in WR galaxies (Schaerer, Contini & Pindao 1999) and metal rich giant HII regions (Pindao et al. 2002). Hence, a NGC 3367-like component diluted to $< 30\%$ of the optical flux yields WR bump equivalent widths of *at most* 1.5 Å, which is comparable to our spectral resolution, so weaker features are unlikely to be detected. The weakness of the young starburst component in LLAGN may thus explain why we have not detected the WR bump in our data.

It is therefore clear that young stellar populations contribute very little to the optical spectra of LLAGN. It is important to point out that even when $< 10^7$ yr stars dominate the UV light, as in NGC 404, NGC 4569, NGC 5055 and NGC 6500 (Maoz et al. 1998), their contribution does not exceed 30% of the λ4020 flux. In fact, these young starbursts are not even detected in the optical for NGC 404 and NGC 5055 due to their *low contrast* with respect to older populations.

While current star formation seems to be proceeding at a residual level in LLAGN, the ubiquity of intermediate age populations indicates that its was much more prominent 10^8–10^9 yr ago, which points to a time-decaying star formation activity. This result contrasts with that obtained for studies of type 2 Seyferts, where young stellar populations are found in abundance (eg, Cid Fernandes et al. 2001a; Joguet et al. 2001). The mean age of stars in

the central regions of Seyfert 2s is thus smaller than that in LLAGN. It is equally instructive to compare the stellar populations of weak and strong-[OI] LLAGN. The finding that intermediate age populations are found almost exclusively among weak-[OI] nuclei implies that these sources are on-average younger than those with strong [OI] emission. The implications of these results for evolutionary scenarios are considered in §**??** and Paper II.

5. Spectral Properties

In this section we present measurements of a suite of stellar features in the nuclear spectra presented above. Measurements through the HFS aperture discussed in §**??** are only used here for comparison purposes. Tables with these and other measurements not published here are available upon request.

5.1. Equivalent widths and colors in Bica's system

In a series of papers starting in the mid 80's, Bica & co-workers have explored a stellar population synthesis technique known as Empirical Population Synthesis (EPS), which decomposes a given galaxy spectrum in a combination of observed spectra of star clusters. In practice, instead of modeling the F_λ spectrum directly, this method synthesizes a number of absorption line equivalent widths (W_λ) and continuum colors (C_λ), which are used as a compact representation of F_λ. EPS has proven a very useful tool in the analysis of galaxy spectra in a variety of contexts, from normal galaxies (Bica 1988), to starbursts (Raimann et al. 2000; Cid Fernandes, Leão, Rodrigues-Lacerda 2003) and even AGN (Schmitt, Storchi-Bergmann & Cid Fernandes 1999; Raimann et al. 2003).

In this section we present measurements of W_λ and C_λ in Bica's system. These will be used here as a raw measures of stellar population characteristics in our sample galaxies. These same data are used in Paper II as input for an EPS analysis. As a side-step to this investigation, we have developed a fully automated scheme to measure W_λ and C_λ in this system. This is discussed next.

5.1.1. Automated measure of the Pseudo Continuum

A drawback of Bica's system is its subjectivity. Both equivalent widths and colors are measured relative to a *pseudo continuum* (PC_λ), defined at pre-selected pivot wavelengths, which is traced interactively over the observed spectrum (see Cid Fernandes et al. 1998 for

an illustrated discussion). Historically, this has limited the use of EPS to a small number of researchers initiated in the "art" of drawing this continuum. Furthermore, the lack of an objective recipe to define PC_λ makes this whole system useless in face of the huge spectral databases currently available, which must be processed in an entirely automated manner. The present data set is itself an example: Counting all nuclear and off-nuclear extractions, there are over 700 spectra.

In order to remedy this situation, we have formulated an *a posteriori* definition of Bica's system. This was done by means of a straightforward computational procedure which mimics the placement of the pseudo continuum, which until now has been carried out by hand.

We started by measuring by hand a representative sub-set of 42 spectra in the current data set, all normalized to the respective median flux in the 4789–4839 Å interval. For each pivot wavelength λ we have then computed *median* fluxes in windows of different sizes and locations. Windows were restricted to be at least 10 Å wide and centered within 100 Å of the corresponding pivot λ. The manually measured PC_λ fluxes were then compared to the automatically measured median fluxes (MF_λ) for all spectra, and a linear relation

$$PC_\lambda = a_\lambda + b_\lambda MF_\lambda \tag{1}$$

was fitted using an ordinary least squares. The optimal window size and location where chosen to be those which produced the best linear correlation coefficient (ie, smallest residuals). Window parameters and the corresponding MF_λ to PC_λ conversion coefficients a_λ and b_λ are listed in Table **??** for six pivot λ's used in this work: 3660, 3780, 4020, 4510, 4630 and 5313 Å.

Table 4. Window definitions for the Pseudo Continuum

Pivot λ [Å]	Interval [Å]	a_λ^1	b_λ
3660	3657–3667	0.0165	1.0069
3780	3775–3785	0.0130	1.0274
4020	4009–4020	0.0161	1.0019
4510	4501–4512	0.0820	0.9337
4630	4609–4627	0.1072	0.9037
5313	5307–5317	-0.0437	1.0507

[1]The coefficient a_λ is in units of the median flux in the 4789–4839 Å interval used to normalize the spectra. b_λ is adimensional

This recipe works extremely well, with linear correlation coefficients above $r = 0.97$ for all λ's. Differences between manual and automated PC_λ measurements in our training set of 42 galaxies are of order 3%. This is well within the level of agreement between manual measurements of PC_λ carried out by different people (Cid Fernandes et al. 1998). We have further verified that the inclusion of other terms in equation (**??**) does not improve the fits significantly. Figure **??** illustrates the pseudo continuum, as measured through our objective system. Equivalent widths are measured with respect to the continuum formed by linear interpolation between the PC_λ pivot points. The differences between W_λ measured with manual and automatic PC_λ is also of order 3%, being always smaller than 0.5 Å.

We thus conclude that we have succeeded in formulating a non-subjective definition of the pseudo continuum (and hence equivalent widths) in Bica's system, thus overcoming a long held objection to this measurement system.

5.1.2. Results

We have measured 7 equivalent widths in Bica's system: W_C, W_{wlb}, W_K, W_H, W_{CN}, W_G and W_{Mg}. The window definitions for these absorption features are the same defined in previous works (Bica & Alloin 1986; Bica, Alloin & Schmidt 1994). Note that W_C is actually centered in a continuum region just to the blue of H9. In old populations, the spectrum in this region is well bellow the pseudo continuum due to a multitude of weak metal lines, yielding $W_C \sim$ 4–5 Å (eg., NGC 266 and NGC 521 in Figure **??**). For populations of ~ 1 Gyr or less, the continuum raises and W_C approaches 0, as seen in NGC 4150 and NGC 4569 (Figure **??**). For our sample, this index is a useful tracer of the presence or HOBLs. All cases where the HOBLs are visually obvious have $W_C < 3$ Å, while objects with $W_C > 4$ Å show no sign of these features. W_{wlb} (where "wlb" stands for "weak line blend") is centered on H9, but has a large value (similar to the CaII K line, W_K) even in the absence of H9 because of the blend of many weak metal lines. Detailed discussions on the properties of these indices can be found in Bica et al. (1994) and Storchi-Bergmann et al. (2000).

In Table **??** we present the results for our nuclear spectra. The continuum colors PC_{3660}/PC_{4020} and PC_{4510}/PC_{4020}, corrected for Galactic extinction, are also listed. The uncertainties in all these spectral indices were estimated by means of Monte Carlo simulations. Each spectrum was perturbed 1000 times with Gaussian noise with amplitude equal to the rms fluctuation in the 4010–4060 Å interval. All indices were measured for each realization of the noise, and the 1σ uncertainties were computed from the dispersion among the 1000 perturbed spectra. The median uncertainties are between 0.3 and 0.5 Å for all W_λ's and 0.03 for the PC_{3660}/PC_{4020} and PC_{4510}/PC_{4020} colors. The largest uncertainties are not

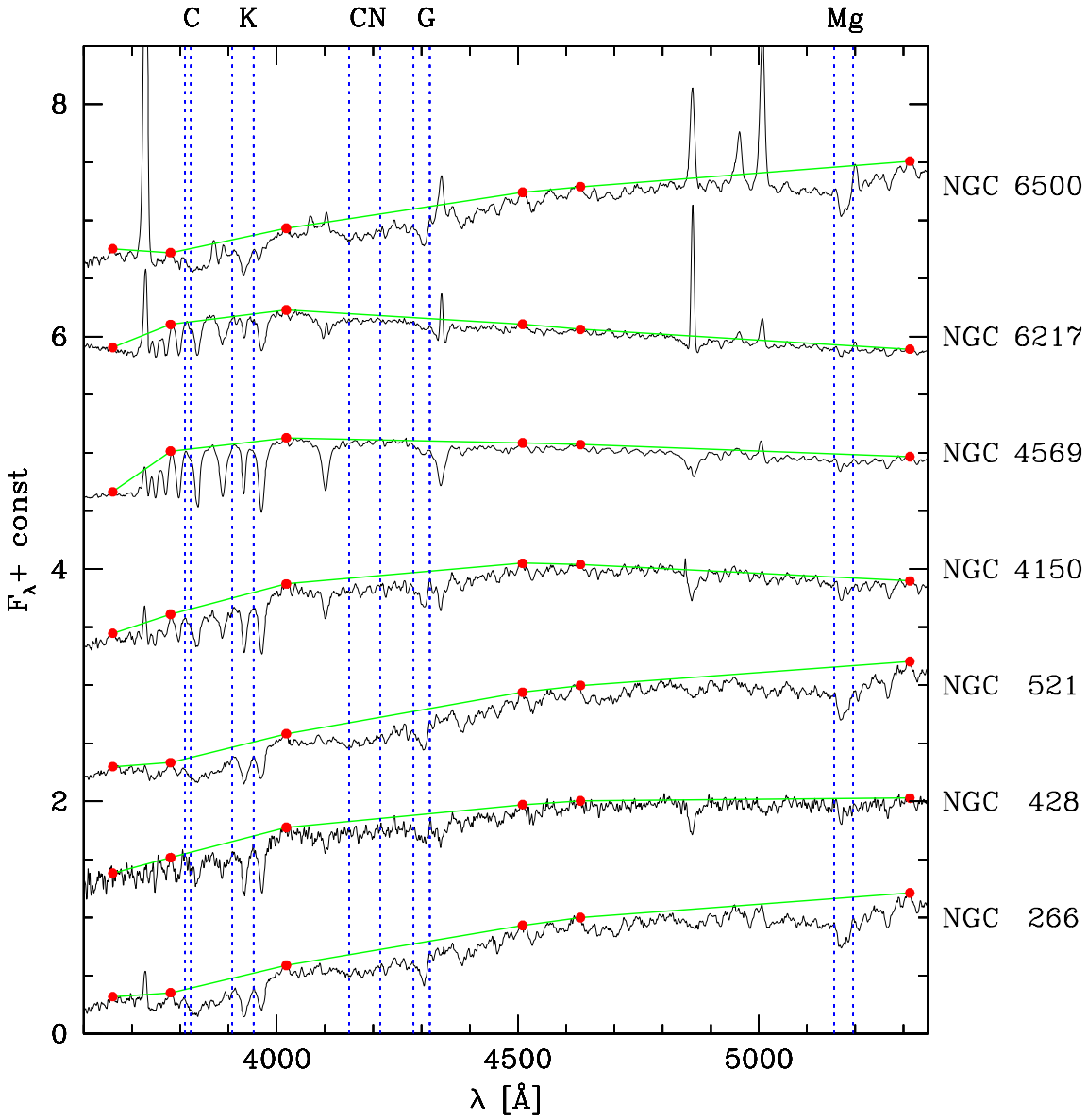

Fig. 10.— Examples of the pseudo continuum in Bica's system, traced by the automatic method developed here (see text). Solid dots mark the pivot continuum points. Vertical dotted lines indicate windows of integration of some of the absorption features in this system. From left to right: W_C, W_K, W_{CN}, W_G and W_{Mg}.

more than twice these values.

In Figure **??** we illustrate the relation between the $\eta = Y$, I, I/O and O empirical stellar population classes defined in §**??** and the equivalents widths W_C, W_K, W_G, W_{Mg} and the PC_{4510}/PC_{4020} color. The correspondence is excellent, as can be appreciated by the locations of different symbols in all panels in this figure. Nuclei with young or intermediate age populations are confined to the low W_λ and blue color bottom-left corners of Figures **??**a–d, while nuclei dominated by old stars populate the high W_λ, red region, with $\eta = I/O$ objects in between. Approximate dividing lines can be placed at $W_C = 3.5$, $W_K = 15$ $W_G = 9$, $W_{Mg} = 9$ Å and $PC_{4510}/PC_{4020} = 1.55$.

Any of the W_λ's in Figure **??** can therefore be used as a continuous stellar population tracer which replaces our discrete I, I/O, O classification. In our previous study of the stellar populations in type 2 Seyferts (Cid Fernandes et al. 2001a) W_K was used in this way. Of all absorption features measured here, W_K is the strongest one, which makes it also the more precise in relative terms. Although the K line is actually produced by late type stars, it indirectly traces younger populations by the dilution they cause on W_K. For this reason, in practice W_K is nearly as good a tracer of HOBLs as a more direct measure of these features, like W_C (Figure **??**a).

5.2. Spectral Properties in HFS's system

HFS97 used a set of spectral indices (defined by Whorthey 1992 and Held & Mould 1994) which also allow a characterization of stellar populations. Seven of the nine absorption equivalent widths and one of the two colors measured by HFS97 are in the wavelength range covered by our data: the G-band, Hγ, Fe4383, Ca4455, Fe4531, Fe4668, Hβ and $c(44-49)$. We have measured these indices in our spectra following the recipes in HFS97. This was done mainly for comparison purposes.

In Figure **??**a we compare the equivalent width of the G-band for our HFS-aperture spectra with the measurements of HFS97. The mean difference is just 0.03 Å, and the rms is 0.6 Å, within the measurement errors of both studies. Similarly, Figure **??**b compares the values of $c(44-49)$ in these two studies. The difference in $c(44-49)$ is just 0.03 ± 0.04, again within the errors.

In Figure **??**c we compare the equivalent widths of the G band as measured in the HFS system and Bica's W_G, while in Figure **??**d we plot the $c(44-49)$ color against Bica's W_K. All quantities are measured from our nuclear spectra. The relatively tight relations between these independent measurements reinforces the impression from Figure **??** that different

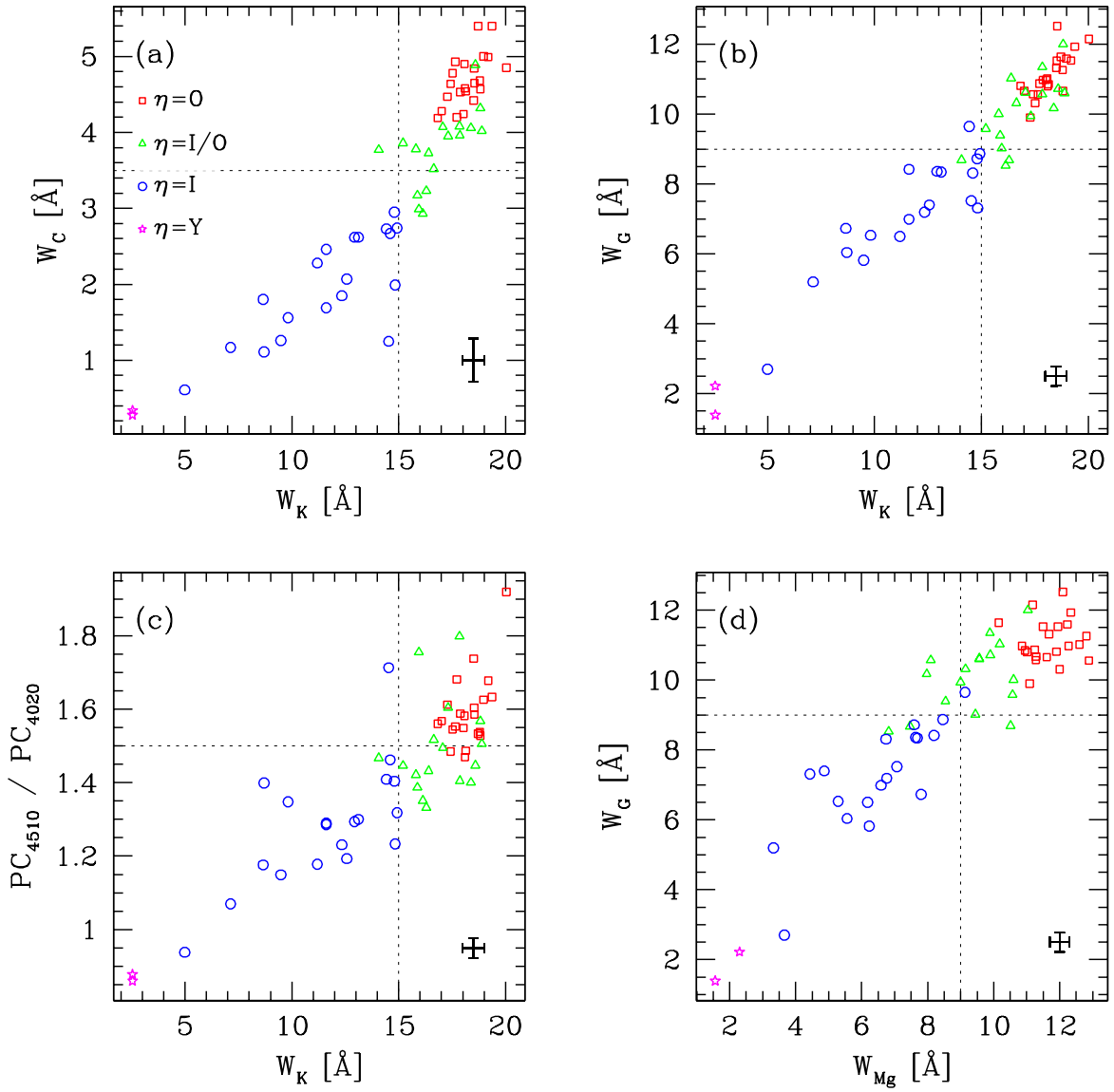

Fig. 11.— Relations between the equivalent widths of four absorption lines and one color in Bica's system. Empirical stellar population classes Y, I, I/O and O are represented by different symbols. Squares, triangles, circles and stars represent $\eta = O$, I/O, I and Y respectively. (The two stars correspond to NGC 3367 and NGC 6217, two Starburst nuclei in our comparison sample.) Dotted lines approximately separate classes $\eta = Y$ and I from $\eta = I/O$ and O. Mean error bars are indicated in the bottom right corner of the figures.

Table 5. Nuclear Spectral Properties

Galaxy	W_C	W_{wlb}	W_K	W_H	W_{CN}	W_G	W_{Mg}	$\frac{F_{3660}}{F_{4020}}$	$\frac{F_{4510}}{F_{4020}}$	$D_n(4000)$	Hδ_A	W(O II)
NGC 0266	4.6	18.0	18.8	13.5	15.7	10.7	11.6	0.55	1.53	2.03	-2.1	5.4
NGC 0315	4.3	17.4	17.0	11.7	15.1	10.7	11.3	0.63	1.57	2.00	-2.8	8.1
NGC 0404	1.6	9.6	9.8	11.3	7.4	6.5	5.3	0.44	1.35	1.50	4.5	9.9
NGC 0410	4.9	19.4	17.6	12.9	17.6	10.6	12.9	0.60	1.55	2.13	-3.1	-1.0
NGC 0428	2.0	10.9	14.8	12.6	8.5	7.3	4.4	0.49	1.23	1.65	2.4	-1.7
NGC 0521	4.5	18.1	17.9	13.4	17.4	11.0	12.3	0.52	1.59	2.01	-2.7	-1.3
NGC 0660	1.3	10.8	14.5	11.5	7.3	7.5	7.1	0.47	1.71	1.72	-1.4	22.4
NGC 0718	2.6	13.1	13.1	12.9	9.5	8.3	7.7	0.52	1.30	1.65	3.1	1.0
NGC 0772	2.5	10.5	11.6	10.0	11.0	8.4	8.2	0.68	1.29	1.46	-0.3	0.8
NGC 0841	2.7	13.5	14.9	13.0	10.4	8.9	8.5	0.55	1.32	1.73	1.9	1.7
NGC 1052	4.5	15.8	17.3	8.2	18.1	9.9	11.1	0.63	1.61	1.88	-1.3	87.5
NGC 1161	5.0	19.4	19.0	13.8	18.5	11.6	12.2	0.56	1.63	2.16	-2.8	-1.7
NGC 1169	4.3	16.7	18.8	12.8	15.5	12.0	11.0	0.61	1.57	2.08	-2.4	7.3
NGC 2681	1.8	11.5	12.3	12.8	8.3	7.2	6.8	0.47	1.23	1.57	4.9	1.6
NGC 2685	5.4	17.6	18.7	13.6	15.0	11.6	10.1	0.55	1.53	2.01	-1.9	0.6
NGC 2911	4.2	18.4	17.7	13.5	17.7	10.9	11.2	0.51	1.68	2.05	-2.0	29.1
NGC 3166	3.2	15.2	15.9	13.0	12.1	9.4	8.5	0.53	1.39	1.80	0.8	4.7
NGC 3169	4.0	16.6	17.3	13.3	12.9	9.9	9.0	0.50	1.60	1.99	-0.4	6.2
NGC 3226	4.4	18.2	18.5	13.4	17.6	11.3	11.7	0.58	1.74	2.13	-2.4	7.7
NGC 3245	3.9	15.3	15.2	11.8	12.7	9.6	10.6	0.67	1.45	1.79	-1.5	1.7
NGC 3627	1.7	11.6	11.6	12.7	7.0	7.0	6.6	0.48	1.29	1.55	4.4	7.8
NGC 3705	3.0	12.9	14.8	13.1	10.1	8.7	7.6	0.49	1.40	1.73	2.2	4.0
NGC 4150	2.1	11.2	12.6	12.3	7.7	7.4	4.9	0.51	1.19	1.55	3.6	2.3
NGC 4192	3.0	15.3	16.0	10.9	11.8	9.0	9.5	0.53	1.76	1.93	0.1	13.4
NGC 4438	4.1	17.4	17.9	12.6	15.7	11.4	9.9	0.51	1.80	2.00	-1.9	57.8
NGC 4569	0.6	7.4	5.0	9.5	1.5	2.7	3.7	0.60	0.94	1.21	6.4	1.2
NGC 4736	2.6	13.6	12.9	12.3	9.9	8.4	7.6	0.53	1.29	1.67	2.8	-0.1
NGC 4826	2.7	15.2	14.4	12.7	13.2	9.6	9.1	0.52	1.41	1.76	1.0	4.6
NGC 5005	2.7	13.8	14.6	12.1	10.6	8.3	6.7	0.48	1.46	1.74	2.3	38.1
NGC 5055	3.8	15.1	14.1	11.9	15.1	8.7	10.5	0.54	1.47	1.75	-0.9	-1.3
NGC 5377	1.8	10.7	8.7	11.0	8.0	6.7	7.8	0.53	1.18	1.45	3.7	4.0
NGC 5678	1.1	7.8	8.7	10.3	3.8	6.0	5.6	0.49	1.40	1.48	3.6	-0.1
NGC 5879	3.2	11.7	16.3	12.7	8.8	8.7	7.5	0.48	1.33	1.72	0.8	3.2
NGC 5921	2.3	11.2	11.2	11.6	6.5	6.5	6.2	0.53	1.18	1.51	4.6	5.0
NGC 5970	4.1	14.5	18.4	13.3	10.1	10.2	8.0	0.61	1.40	1.86	-0.8	-2.5
NGC 5982	4.6	18.4	18.1	13.7	16.1	10.8	11.0	0.57	1.47	2.05	-1.9	-2.5
NGC 5985	4.0	15.5	18.9	12.1	13.2	10.6	9.6	0.59	1.51	1.97	-2.6	25.8
NGC 6340	4.9	18.1	20.0	14.3	17.1	12.1	11.2	0.49	1.92	2.26	-2.5	2.4
NGC 6384	4.9	15.2	18.6	12.9	10.3	10.7	9.9	0.66	1.45	1.92	-2.3	-2.7
NGC 6482	4.7	18.7	18.8	13.4	17.5	11.3	12.8	0.63	1.54	2.11	-2.7	4.4
NGC 6500	3.8	14.5	15.8	8.7	14.5	10.0	10.6	0.74	1.42	1.74	-4.3	98.2
NGC 6501	4.2	17.7	16.8	12.9	17.7	10.8	11.9	0.56	1.56	2.03	-2.2	-3.4
NGC 6503	1.3	7.9	9.5	10.4	4.3	5.8	6.2	0.67	1.15	1.36	2.9	4.5
NGC 6702	4.5	18.5	18.1	13.3	14.0	10.8	11.0	0.61	1.49	2.04	-1.7	-3.0
NGC 6703	4.8	18.7	18.5	13.8	16.3	11.5	11.5	0.56	1.60	2.11	-2.4	-1.9
NGC 6951	3.7	14.1	16.4	11.7	15.7	11.0	10.2	0.52	1.43	1.70	-0.2	21.3
NGC 7177	3.5	14.5	16.6	12.5	11.7	10.3	9.2	0.58	1.52	1.80	-1.3	11.2
NGC 7217	5.0	18.7	19.2	14.0	17.2	11.5	12.0	0.53	1.68	2.07	-2.6	12.2
NGC 7331	4.2	16.8	18.0	13.6	15.3	11.0	10.9	0.54	1.55	1.99	-1.0	-1.0
NGC 7626	4.9	19.2	18.1	13.9	17.9	11.0	12.6	0.58	1.58	2.12	-3.3	-1.2
NGC 7742	4.1	15.9	17.1	13.1	13.1	10.6	9.6	0.52	1.50	1.90	-0.9	2.2
NGC 3367	0.3	1.8	2.6	1.1	1.5	1.4	1.6	1.07	0.86	1.05	-3.0	13.3
NGC 6217	0.3	3.9	2.5	5.3	2.7	2.2	2.3	0.75	0.88	1.13	3.1	5.9
NGC 0205	1.2	8.4	7.1	11.5	4.3	5.2	3.3	0.51	1.07	1.37	6.3	-2.0
NGC 0221	4.0	15.5	17.9	13.9	11.9	10.6	8.1	0.60	1.41	1.86	-0.9	-3.4
NGC 0224	4.8	18.6	17.5	13.7	18.5	10.3	12.0	0.63	1.54	2.06	-2.9	-4.1
NGC 0628	2.9	13.1	16.1	12.7	8.5	8.5	6.8	0.64	1.35	1.74	0.5	-2.4
NGC 1023	5.4	20.8	19.4	14.5	19.1	11.9	12.3	0.57	1.63	2.26	-3.7	-4.6
NGC 2950	4.6	18.7	17.4	13.2	17.0	10.6	11.3	0.59	1.48	2.04	-2.0	-3.0
NGC 6654	4.7	16.4	18.5	13.4	16.6	12.5	12.1	0.61	1.58	2.09	-1.6	-5.4

Note. — Col. (1): Galaxy name; Cols. (2–10): Equivalent widths of seven absorption features and two colors, all in Bica's system. Col. (11): 4000 Å break index (Balogh et al. 1999). Col. (12): Hδ_A equivalent width of Worthey & Ottaviani (1997). Col. (13): [OII] equivalent width of Balogh et al. (1999). All equivalent widths are given in Å

stellar indices in galaxy spectra are highly correlated. A corollary of these correlations is that a single index (say, W_K) is enough to provide a good first order characterization of the stellar populations in our sample galaxies. This relatively high degree of redundancy in galaxy spectra is also detected by studies of principal component analysis (e.g., Schmidt et al. 1991; Sodré & Cuevas 1997), which show that a large fraction of the variance in galactic spectra is described by a single principal component. The physical property behind such an approximately mono-parametric behavior is the *age* of the dominant stellar population (Schmidt et al. 1991; Ronen, Aragon-Salamanca & Lahav 1999).

The strong inter-relations between different stellar population indices can be used to extend results drawn from our sample to the full HFS sample. For instance, any correlation found between W_C or W_K and emission line properties for our galaxies will also appear with the W(G-band) HFS index, which has been measured by HFS97 for most of their 162 LLAGN. Analogously, statistics related to our Y, I, I/O and O stellar population classes can be readily extended to the full HFS sample exploring the relation between η and, say, W(G-band).

5.3. Other spectral indices: $D_n(4000)$, Hδ_A and W(O II)

Besides the CaII K line and the HOBLs, the interval between 3500 and 4200 Å contains other features of interest. The 4000 Å break and Hδ, for instance, have been recently used as stellar population diagnostics for SDSS spectra of both normal and active galaxies (Kauffman et al. 2002, 2003). We have measured these two indices for our spectra following the Balogh et al. (1999) definition of $D_n(4000)$ and the Worthey & Ottaviani (1997) definition of Hδ_A. These are the same indices used in the SDSS work. We have not corrected Hδ_A for emission as this is insignificant for most of our LLAGN. We further measured the [OII] equivalent width W(O II) according to the recipe of Balogh et al. (1999). All spectra were corrected for Galactic reddening prior to these measurements.

These indices are listed in the last three columns of Table **??**. Note that H$\delta_A > 0$ corresponds to absorption while W(O II) > 0 corresponds to emission. Note also that negative W(O II) is obtained in many cases, but this does not necessarily means a non-detection of [OII]. For instance, [OII] is clearly seen in the starlight subtracted spectrum of NGC 7626, while the W(O II) index, which is measured over the total spectrum, yields -1.2 Å. As for other emission lines in LLAGN, the accurate measurement of [OII] requires a careful starlight subtraction.

In Figure **??**a we examine the relation between $D_n(4000)$ and Hδ_A. The global distri-

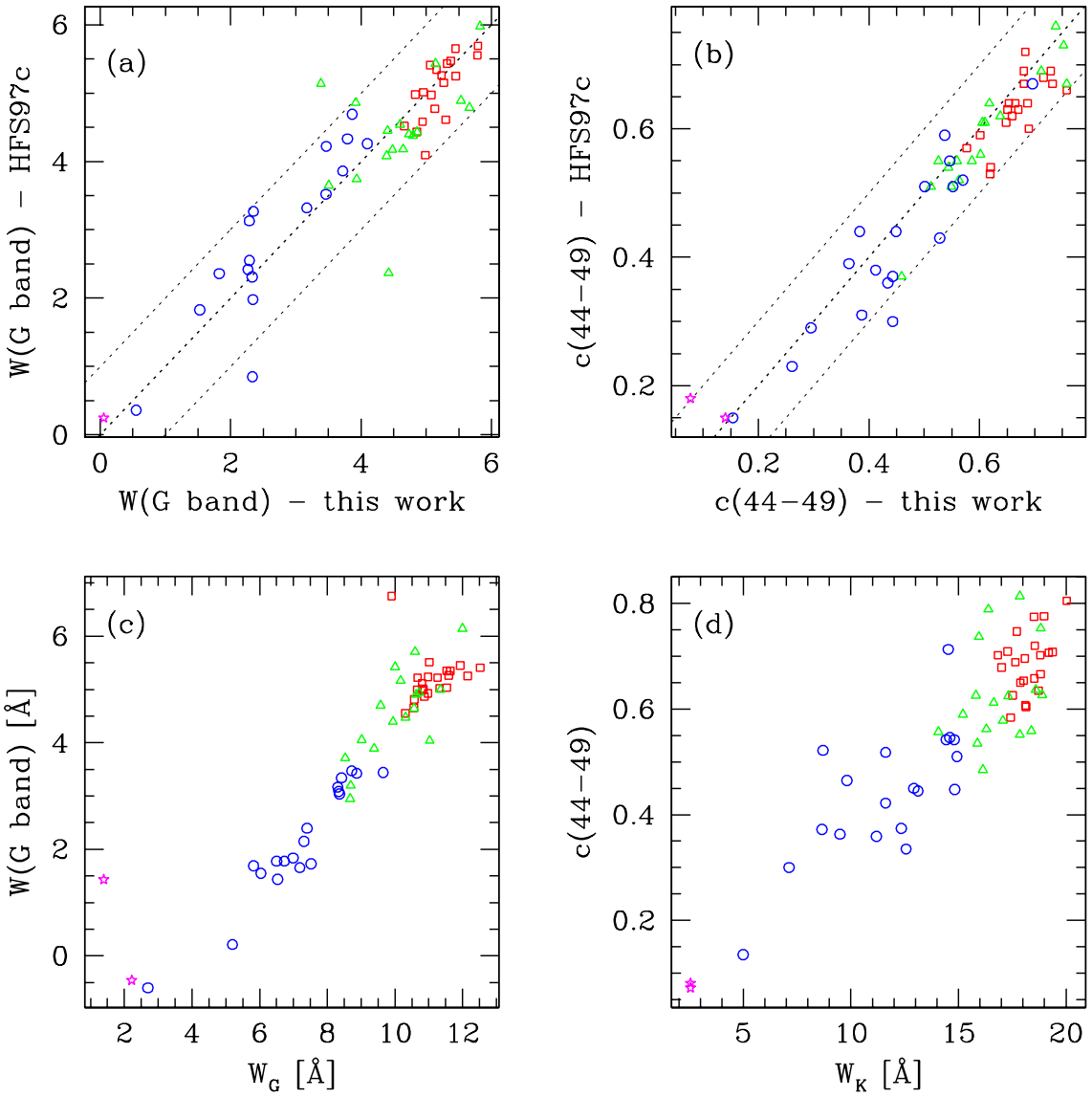

Fig. 12.— *Top:* (a) Comparison of the equivalent width of the G band and (b) the $c(44-49)$ color for our HFS-aperture spectra and the measurements of HFS97. Both indices were computed according to the definitions in HFS97. Diagonal lines indicate $y = x$ and the ± 2 sigma range. *Bottom:* Relation between W_G and W_K, measured through Bica's system, and two HFS indices: (c) the G-band equivalent width and (d) $c(44-49)$. Symbols as in Figure **??**.

bution of LLAGN in this diagram is similar to that obtained for SDSS galaxies (Kaufmman et al. 2002). Interestingly, our $\eta = I$ LLAGN, which are nearly all weak-[OI] sources, lie above the locus of steady star formation models of Kaufmann et al. (2002), in a region occupied by galaxies which have experienced bursts of star formation in the past $\sim 10^9$ yr. This is consistent with the strong HOBLs found in these systems and the considerations of §**??**. The location of $\eta = I$ weak-[OI] sources in Figure **??**a is also similar to that of AGN with $L_{[OIII]} < 10^7$ $L_\odot$ and TO-like emission line ratios in Kauffman et al. (2003). Notwithstanding these similarities, it is important to observe that while the SDSS work pertains to scales of several kpc, our data traces stellar populations on scales of typically 70 pc.

Figure **??**b illustrates the strong relation between Bica's W_K and $D_n(4000)$, which is not surprising given that the W_K window is contained in blue window of $D_n(4000)$. The dashed line indicates the quadratic fit:

$$D_n(4000) = (1.013 \pm 0.006) + (0.031 \pm 0.001)W_K + (0.00124 \pm 0.00007)W_K^2 \qquad (2)$$

6. The Link Between Stellar Population and Emission Line Properties in LLAGN

Several times in §**??** we have noted an apparent connection between stellar population features revealed by our spectroscopy and the weak/strong [OI] classification. In this section we use the spectral properties measured in §**??** in conjunction with the [OI]/Hα ratio from HFS97 to investigate this connection in a quantitative manner.

One way to investigate this relation more closely is to correlate [OI]/Hα with the W_C index, a useful tracer of the presence of HOBLs. The strong tendency of HOBLs to appear preferentially in weak-[OI] nuclei noted in §**??** should reveal itself as a correlation between [OI]/Hα and W_C. Similar correlations should exist between [OI]/Hα and the equivalent widths of metal absorption lines, since HOBLs come with an associated blue continuum which dilutes spectral features like the K line and the G band.

Figure **??** confirms these expectations. The figure plots [OI]/Hα against our nuclear measurements of W_C, W_K, W_G and W_{Mg} (Table **??**). What is seen in these plots is not so much a correlation in the sense of points scattered around a line, but a marked *dichotomy*: Nearly all nuclei with weak absorption lines are weak-[OI] emitters, whereas nuclei with strong metal lines span the full range of [OI]/Hα. In graphical terms, the top-left regions of all panels in Figure **??** are remarkably empty!

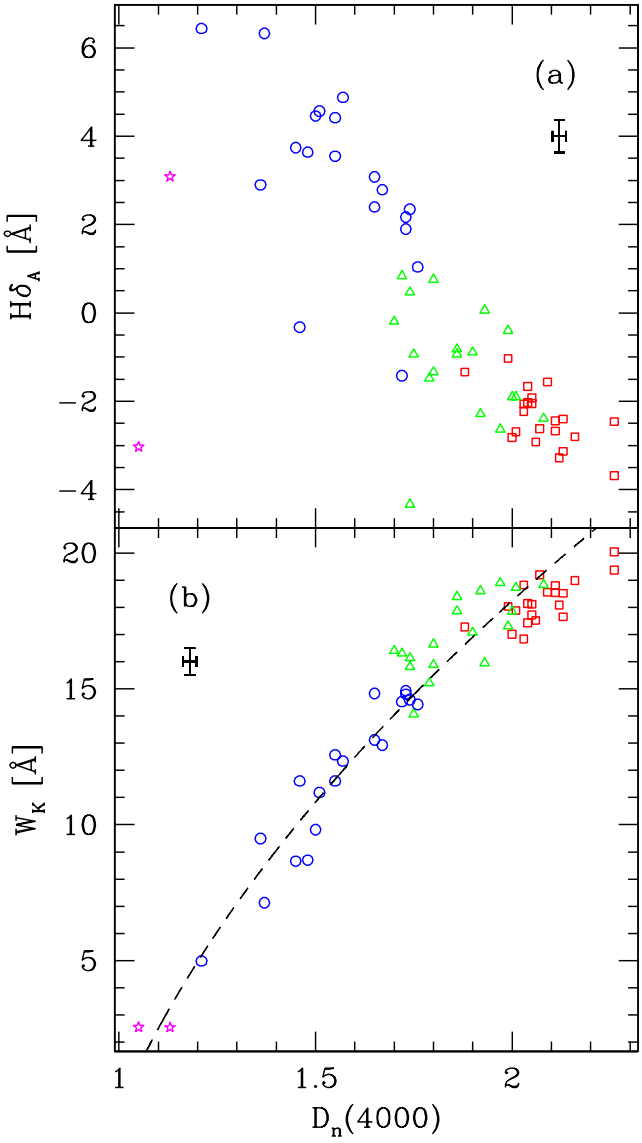

Fig. 13.— Relations between $D_n(4000)$, Hδ_A and W_K. Symbols as in Figure **??**. The dashed line in (b) shows a second order polynomial fit.

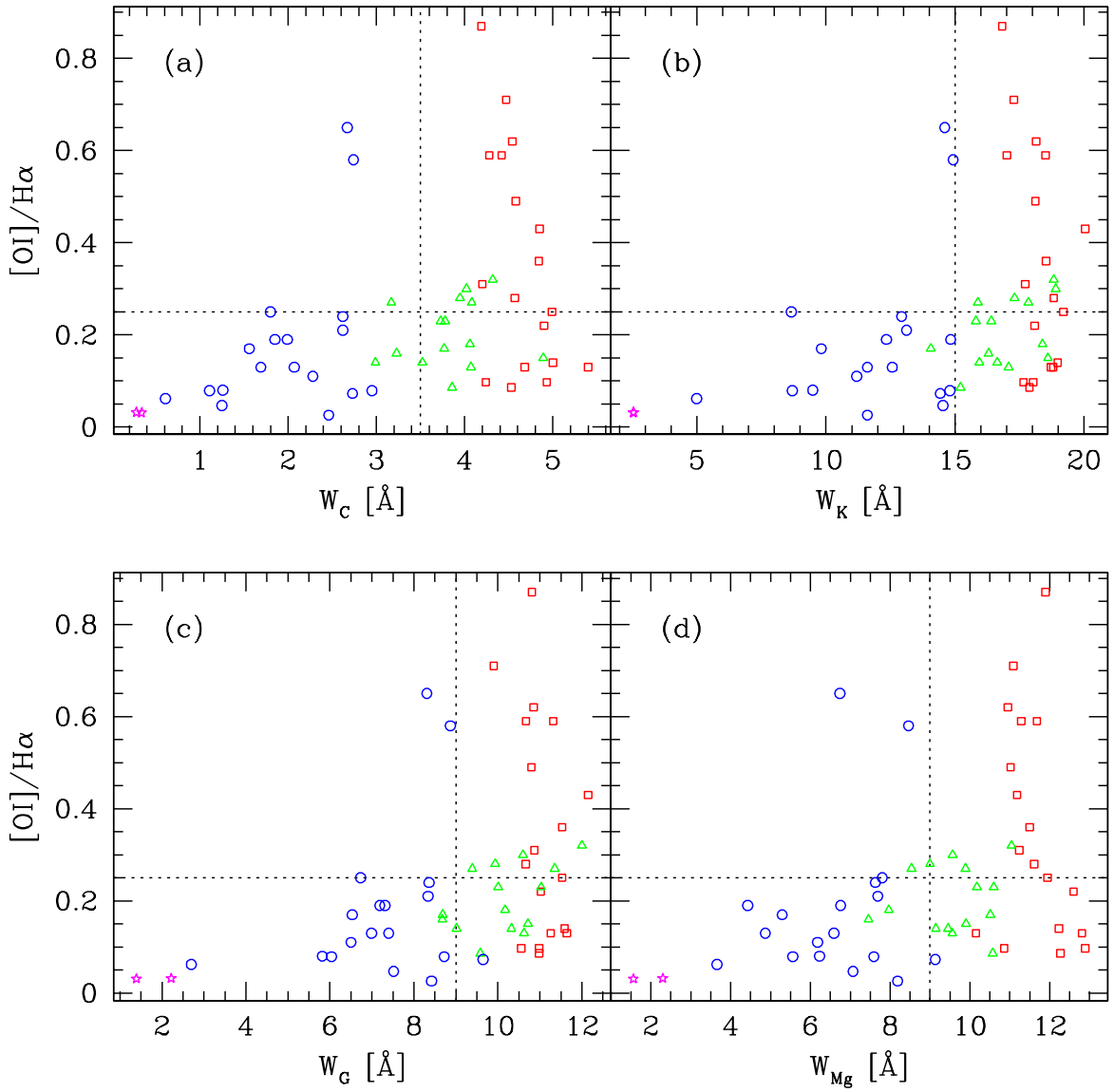

Fig. 14.— Comparison of absorption equivalent widths, which trace stellar populations, with the [OI]/Hα ratio, an AGN indicator. The [OI]/H$\alpha = 0.25$ border-line which separates weak from strong-[OI] nuclei is indicated. The vertical dotted lines are the same as in Figure **??**; they separate objects with a strong intermediate age population ($\eta = I$) from objects dominated by old stars ($\eta = O$). Symbols as in Figure **??**.

This is not the first time in this paper that [OI]/Hα is plotted against a stellar population index. In Figure **??** we plotted [OI]/Hα versus W(G band) for the full HFS sample. There we see the same "inverted L" shape of any of the panels of Figure **??**. Overall, these figures spell out a clear message: The Narrow Line Region of LLAGN evidently knows what value of [OI]/Hα it can or cannot assume for a given stellar W_λ. This finding implies a strong connection between stellar populations and gas excitation processes in LLAGN.

As suggested by the referee, an alternative reading of this result could be that galaxies with important circumnuclear star formation have an excess of Hα emission in the central few arcsec (note that the [OI]/Hα values are from the $2'' \times 4''$ measurements by HFS97), resulting in a lower [OI]/Hα ratio. We have studied the aperture dependence of the Hα flux in order to check whether the link between [OI]/Hα and the stellar population is not a consequence of an excess of Hα flux in the larger HFS97 apertures, compared to the smaller apertures ($1'' \times 1.1''$) used in this work to derive the stellar population properties. We have retrieved from the HST archive STIS (G750M or G750L) spectra of 27 out of the 28 LLAGN analysed in Paper II. We find that Hα is very compact in all strong-[OI] LLAGN. In weak-[OI] LLAGN, the geometry of Hα is more diverse: in 7/22 Hα is compact, and in 14/22 more than 50% of the flux (measured through a $0.2'' \times 4''$ extraction) is inside the central $0.2'' \times 1''$. On the other hand, we find that the extension of the Hα emission does not correlate with the type of nuclear stellar population. In addition, we find that there is no correlation between the Hα luminosity and the [OI]/Hα ratio (both measured by HFS97). We thus conclude that the lower values of [OI]/Hα in weak-[OI] LLAGNs are not due to an excess of Hα emission provided by recent star formation in spatial scales of a few arcsecs.

A compelling visualization of the relation between [OI]/Hα and the stellar population properties is presented in Figure **??**. In this figure we divide objects into bins in stellar W_λ and within each bin we compute the fraction of objects with [OI]/H$\alpha < 0.17$ (filled areas), $0.17 \leq$ [OI]/H$\alpha \leq 0.25$ (hatched areas) and [OI]/H$\alpha > 0.25$ (empty areas). The panels with W_K and W_C are for our sample, while the panel with W(G-band) uses data tabulated in HFS97 for all their LLAGN.

The predominance of weak [OI] emitters among objects with low stellar absorption equivalent widths is obvious to the eye. Of the 19 LLAGN with $W_K < 15$ Å, 17 have [OI]/H$\alpha \leq 0.25$. Similarly 18 of the 21 nuclei with $W_C < 3.5$ Å have [OI]/H$\alpha \leq 0.25$. Hence, $\sim 90\%$ of objects with weak absorption lines are also weak [OI] emitters. Note that the above limits in W_K and W_C correspond approximately to the border line between our $\eta = I$ and $\eta = I/O$ or O stellar population classes (Figure **??**), so nearly identical statistics are obtained comparing η with [OI]/Hα. Likewise, since $\eta = I$ systems are also those with HOBLs, one can alternatively express the above statistics in terms of a [OI]/Hα-HOBLs

connection.

For the full HFS sample, $\sim 80\%$ of the W(G band) < 4.5 Å sources have [OI]/H$\alpha \leq 0.25$ (Figure **??**c). This same fraction results if one uses the HFS97 measurements for the 51 LLAGN in our sample, which reinforces our conclusion that there are no significant differential selection effects between the two samples.

It is important to draw attention to the fact that although most objects with HOBLs and diluted metal lines are weak in [OI], *the converse is not true*. There is a numerous population of weak-[OI] sources *without* conspicuous HOBLs and with stellar population indices typical of old, ~ 10 Gyr populations. Among objects with $W_K > 15$ Å, for instance, $\sim 50\%$ have [OI]/H$\alpha \leq 0.25$. These are the objects located at the bottom-right corners of the "inverted L" distributions in Figures **??** and **??**, also represented by the filled and hatched areas in the large W_λ bins in Figure **??**.

6.1. Interpretation

The shape of the distribution of points in Figure **??**b lends itself to division into four regions, delimited by [OI]/H$\alpha \sim 0.25$ in the vertical (emission line) axis and $W_K \sim 15$ Å in the horizontal (stellar population) axis. Similar divisions can be placed at $W_C \sim 3.5$, $W_G \sim 9$ and $W_{Mg} \sim 9$ Å in the other panels of Figure **??**, and at W(G-band) ~ 4.5 Å in Figure **??**. The top-left of these four quadrants is essentially empty. What kind of objects populate the remaining three quadrants?

Objects with clear signs of stellar populations of $\sim 10^9$ yr or less (ie, those with HOBLs, diluted metal lines and blue colors) all live in the bottom-left quadrant. They are all weak-[OI]'s according to our definition. A plausible reading of this fact is that in these objects stars are directly linked to the gas excitation by some as yet undefined mechanism (see §**??** for a menu of possibilities), resulting in higher Hα per [OI] photon ratio than in strong-[OI] LINERs. These sources could be called *"Young-TOs"*, where "young" actually refers to populations of 10^9 yr of less. Note that the stellar W_λ's in these sources are intermediate between those of starburst and early type galaxies. In other words, they are transition objects also in terms of their stellar populations.

In the opposite end of the [OI]/Hα versus W_λ diagrams, stars cannot play an important role in the gas excitation, since photoionization by hot stars, be they young (ie, a starburst) or old (post-AGB stars), produces smaller values of [OI]/Hα than observed in AGN. The absence of optically significant $\lesssim 10^9$ yr populations corroborates this interpretation. Photoionization by an AGN is likely the dominant emission line mechanism in these sources.

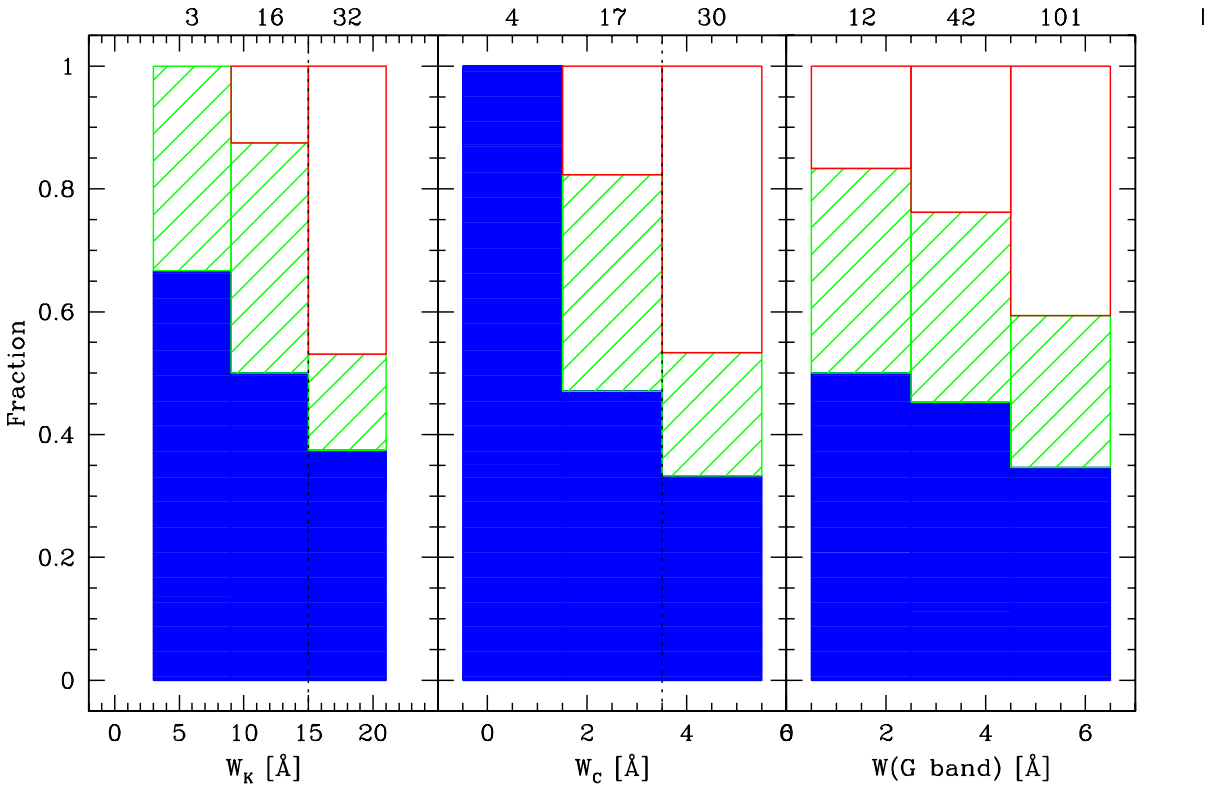

Fig. 15.— Fraction of objects in each of three ranges in [OI]/Hα as a function of different stellar absorption equivalent widths. Filled areas are used for [OI]/H$\alpha < 0.17$, hatched areas for $0.17 \leq$ [OI]/H$\alpha \leq 0.25$ and empty boxes for [OI]/H$\alpha > 0.25$. Numbers at the top indicate the number of objects in each W_λ-bin. The left and middle panels are for the present sample of 51 LLAGN, while the right panel is for the full HFS sample.

Variations in nebular conditions or in the ionizing spectrum can be invoked to explain the range of [OI]/Hα values spanned by the data. A fitting denomination for nuclei in this top-right quadrant is *"Old-LINERs"*.

The bottom right quadrant of Figure **??** is populated by objects with TO-like emission line spectra but no strong optical signs of young or intermediate age stellar populations. These *"Old-TOs"* may well belong to the Old-LINER family, in which case their weak [OI]/Hα should perhaps be explained by an ionizing radiation field softer than for strong-[OI] LINERs. Alternatively, they may be simply weak Young-TOs whose $\lesssim 10^9$ yr stars are completely overwhelmed by the older population. This is likely the case of NGC 5055. The young starburst which clearly dominates the UV light of this galactic nucleus (Maoz et al. 1998) leaves no trace in the optical (Table **??**), although our starlight decomposition indicates that 21% of the 4020 Å flux originates in an intermediate age population. This non-negligible contribution, however, causes little dilution of the metal lines. The lower right quadrant of Figure **??** probably contains other such objects.

To summarize, our results suggest a scenario where stars younger than ~ 1 Gyr somehow participate in the gas ionization of Young-TOs, whereas in Old-LINERs an AGN is the dominant ionizing agent. The situation is less clear for Old-TOs, which may comprise a mixture of the above objects. Interestingly, "Young-LINERs" do not seem to exist. AGN taxonomy surely does not need more sub-classes. Yet, LLAGN have long been known to comprise a heterogeneous class, and, as discussed in §**??**, models involving AGN- and stellar-driven ionization can both explain their emission line properties. This empirically motivated scenario comes in the sense of trying to elucidate which of these two broad physical processes, AGN or stars, best fits a given source. It is equally important to clarify that we do not claim Young-TOs to be AGN-less. After-all, the current common wisdom is that all galaxies with bulges harbor an AGN, be it dead, alive or somewhere in between. In Young-TOs the AGN contribution to the gas ionization would be small. Conversely, ionization by stellar processes in Old LINERs would be overwhelmed by the AGN.

A potential caveat in identifying nuclei with weak metallic lines with stellar processes is that dilution by a quasar-like non-stellar continuum can also produce the same effect. Presumably, this should be more important for type 1 LLAGN, ie, L1.9 and T1.9 in the notation of HFS97. This effect indeed happens in HST spectra of some objects (Paper II). Interestingly, the two objects with W(G band) between 3.5 and 4 Å and [OI]/H$\alpha \sim 0.6$ in Figure **??** which intrude slightly into the "zone of avoidance" are NGC 841 and NGC 5005, both classified as L1.9. Although it is conceivable that this effect operates in a few cases, we find that type 1 and type 2 sources are well mixed in all our diagrams, so this cannot be a major effect in our ground based observations. Furthermore, we point out that HOBLs

were detected in both NGC 841 and NGC 5005, as well as in NGC 2681, another L1.9 with relatively weak metal absorption lines. It therefore seems more likely that the main diluting agent even in these type 1 LLAGN is the continuum associated with stellar populations of $\lesssim 10^9$ yr rather than with a quasar-like continuum.

6.2. Evolution and Contrast

As time passes, HOBLs and the continuum of $\lesssim 10^9$ yr populations gradually disappears, and metal absorption features become progressively stronger. Passive evolution thus moves nuclei in left to right direction in Figures **??** and **??** on time scales of a few Gyr. In the notation of the previous section, objects in the left half of Figures **??** and **??** are nearly all Young TOs. If [OI]/Hα remains constant during this period, stellar evolution would gradually turn a Young-TO onto an Old-TO. This would correspond to a horizontal evolutionary track onto any of our [OI]/Hα versus W_λ diagrams.

However, the hypothesis of constant [OI]/Hα does not seem warranted by the "inverted L" distribution of LLAGN in Figures **??** and **??**, which suggests that the presence of $\lesssim 10^9$ yr populations affects the [OI]/Hα ratio. For didactic purposes, lets consider a situation in which an AGN is entirely responsible for the production of [OI] photons, while Hα is produced both by the AGN and $\lesssim 10^9$ yr stars. In this case the stellar contribution to [OI]/Hα acts just in the denominator of this ratio. Evolution would thus move objects both to the right and upwards along curved mixing lines in Figures **??** and **??** as the stellar powered Hα emission fades. Considering that the AGN part of [OI]/Hα can assume a range of values (due, eg, to different nebular conditions), one arrives at a scenario where stellar evolution takes points in the bottom-left to any possible height in the right part of these figures. In other words, Young-TOs can end up as either Old-TOs or Old-LINERs.

It thus seem plausible that evolution plays a role in defining the looks of LLAGN spectra, both in their stellar and emission lines properties. Physical models for the evolution of [OI]/Hα must bear in mind that the intensity of [OI] is not only driven by the ionizing radiation field; it also depends strongly of the nebular geometry. Thus, variations of the ionization parameter and/or the density structure would also affect the [OI]/Hα ratio. Such variations may be tied to the evolution of stellar populations. In starbursts, for instance, [OI]/Hα is expected to increase with age as the bubble produced by the action of stellar winds and SNe expands (Stasińska, Schaerer & Leitherer 2001; Stasińska & Izotov 2003).

Besides evolution, contrast effects must also be present, as can be illustrated by the case of NGC 6500. Judging by the relative contributions of the Y, I and I/O components

in our starlight decomposition (25, 0 and 4% of the 4020 Å flux, respectively), this is the youngest LLAGN in our sample. Yet, since 71% of the optical light comes from old stars, this galaxy does not quite make it into our observational definition of Young-TO, whereas from the above discussion of evolutionary effects one could naively expect it to be located at the bottom left of our [OI]/Hα versus W_λ diagrams. Further examples of contrast effects are NGC 5055 and NGC 404, whose optical spectra reveal no sign of the young massive stars unambiguously detected at UV wavelengths by Maoz et al. (1998). This starburst component is simply buried under the much stronger contribution of intermediate age and older stars.

A quantitative assessment of these ideas is beyond the scope of this paper. Future communications will explore these issues by means of stellar population synthesis, spectral energy distribution modeling and comparisons to Seyfert and Starburst galaxies.

7. Conclusions

In this paper we presented the first results of a survey of the stellar populations of low luminosity AGN. Nuclear spectra covering the inner ~ 70 pc in radius were presented for 51 LINERs and LINER/HII Transition Objects plus a comparison sample 9 non-active galaxies. The stellar population properties of LLAGN were quantified by means of a comparison with non-active galaxies as well as by measurement of a suite of spectral indices over the 3500–5500 Å interval.

Our main results can be summarized as follows:

1. Young, $< 10^7$ yr starbursts contribute very little to the optical spectrum of LLAGN. Even in the few nuclei known from UV observations to contain young massive stars, these populations participate with no more than 30% of the optical continuum light, and sometimes are altogether undetected due to a much stronger contribution from other stellar populations.

2. Intermediate age, 10^8–10^9 yr populations, on the other hand, are found in at least 1/3 of all LLAGN. These populations are easily characterized by pronounced HI Balmer lines in absorption, diluted metal lines and relatively blue colors.

3. We found a very strong empirical connection between the stellar populations and emission line properties of LLAGN. Nearly all nuclei containing substantial populations of young and/or intermediate age stars are weak [OI] emitters, with [OI]/H$\alpha \leq 0.25$, whereas only $\sim 10\%$ of the sources with stronger [OI] contain such populations. The

mean stellar age of weak-[OI] LLAGN is thus several Gyr younger than that of strong-[OI] LLAGN. Nuclei dominated by older stars, however, span the full range of [OI]/Hα values, from TOs to LINERs.

4. Given a few Gyr, TOs with conspicuous intermediate age populations will naturally evolve to either "Old-TOs" or "Old-LINERs".

Perhaps the major lesson from this study is that the information contained in the stellar populations of active galaxies can provide valuable clues on the nature of these systems. Combining this information with emission line data, we were able to establish an inequivocal connection between stellar populations and the gas excitation mechanism in LLAGN. The physical origin of this connection, however, has not been unveiled in this work. By analogy with previous investigations (particularly of type 2 Seyferts), starburst activity is the prime contender to explain the relation between [OI]/Hα and stellar population properties reported in this work. Direct evidence for young stars in LLAGN is nevertheless too scant to fully subscribe this interpretation at this stage, specially because other scenarios (such as SN shocks and photoionization by evolved post-starburst populations) may potentially explain our findings. Future papers in this series will address these and other related issues exploring complementary spectroscopic and imaging data, as well as detailed modeling of the stellar populations in these sources.

It is a pleasure to thank Grazyna Stasińska, Luis Colina and Áurea Garcia for their enlightening comments and suggestions, and the referee for her/his suggestions that help to improve the paper. RCF and TSB acknowledge the support from CNPq and CAPES. RGD and EP acknowledge support by Spanish Ministry of Science and Technology (MCYT) through grant AYA-2001-3939-C03-01. The data presented here have been taken using ALFOSC, which is owned by the Instituto de Astrofísica de Andalucía (IAA) and operated at the Nordic Optical Telescope under agreement between IAA and the NBIfAFG of the Astronomical Observatory of Copenhagen. We are very grateful to the IAA director for the allocation of 5.5 nights of the ALFOSC guaranteed time. The National Radio Astronomy Observatory is a facility of the National Science Foundation operated under cooperative agreement by Associated Universities, Inc.

REFERENCES

Balogh, M. L., Morris, S. L., Yee, H. K. C., Carlberg, R. G., Ellingson, E. 1999, ApJ, 527, 54

Barth, A. J., Reichert, G. A., Ho, L. C., Shields, J. C., Filippenko, A. V., & Puchnarewicz, E. M. 1997, AJ, 114, 2313

Barth, A. J. & Shields, J. C. 2000, PASP, 112, 753

Barth, A. J. 2002, ASP Conference Series, 258, 147

Bica, E. & Alloin, D. 1986, A&A, 166, 83

Bica, E. 1988, A&A, 195, 76

Bica, E., Alloin, D. & Schmitt, H. R. 1994, A&A, 283, 805

Binette, L., Magris, C. G., Stasińska, G., Bruzual, A. G. 1994, A&A, 292, 13

Bower, G. A., Wilson, A. S., Heckman, T. M.; Richstone, D. O.1996, AJ, 111, 1901

Cardelli, J. A., Clayton, G. C. & Mathis, J. S. 1989, ApJ, 345, 245

Cid Fernandes, R. Jr., Storchi-Bergmann, T. & Schmitt, H. R.1998, MNRAS, 297, 579

Cid Fernandes, R., Heckman, T., Schmitt, H., González Delgado, R.M., Storchi-Bergmann, T. 2001a, ApJ, 558, 81

Cid Fernandes, R., Sodré, L., Schmitt, H., Leo, J. R. S. 2001b, MNRAS, 325, 60

Cid Fernandes, R., Leo, J. R. S. & Rodrigues-Lacerda, R. 2003, MNRAS, 340, 29

Colina, L., González Delgado, R., Mas-Hesse, J. M., Leitherer, C. 2002, ApJ, 579, 545

Donahue, M. & Voit, G. M. 1991, 381, 361

Dopita, M. A. & Sutherland, R. S. 1995, 455, 468

Engelbracht, C. W., Rieke, M. J., Rieke, G. H., Kelly, D. M., Achtermann, J. M. 1998, ApJ, 505, 639

Falcke, H., Nagar, N. M., Wilson, A. S., Ulvestad, J. S. 2000, ApJ, 542, 197

Ferland, G. J. & Netzer, H. 1983, ApJ, 264, 105

Filippenko, A. V. 1996, ASP Conf. Series, 17

Filippenko, A. V. & Terlevich, R. 1992, ApJ, 397, L79

Gonçalves, A. C.; Véron-Cetty, M.-P.; Véron, P. 1999, A&AS, 341, 662

González Delgado, R. M., Heckman, T., Leitherer, C., Meurer, G., Krolik, J., Wilson, A. S., Kinney, S., Koratkar, A.1998, ApJ, 505, 174

González Delgado, R. M., Heckman, T., Leitherer, C. 2001, ApJ, 546, 845

González Delgado, R. M., Cid Fernandes, R., Storchi Bergmann, T., Schmitt, H., Martins, L. P., Pérez, E. J., Leitherer, C., R., Heckman, T. M. 2003, ApJ, submitted (Paper II)

Halpern, J. P. & Steiner, J. E. 1983, ApJ, 269, 37

Heckman, T. M. 1980, A&A, 87, 152

Heckman, T. M., Armus, L. & Miley, G. K. 1990, ApJS, 74, 833

Heckman, T. M., Baum, S. A., van Breugel, W. J. M., McCarthy, P. 1989, ApJ, 338, 48

Heckman, T. M., González-Delgado, R., Leitherer, C., Meurer, G. R., Krolik, J., Wilson, A. S., Koratkar, A., Kinney, A. 1997, ApJ, 482, 114

Held, E. V. & Mould, J. R. 1994, AJ, 107, 1307

Ho, L. C., Filippenko, A. V. & Sargent, W. L. W. 1995, ApJ, 98, 477

Ho, L. C., Filippenko, A. V. & Sargent, W. L. W. 1997, ApJS, 112, 315

Ho, L. C., Filippenko, A. V. & Sargent, W. L. W. 2003, ApJ, 583, 159

Ho, L. C. et al. 2001, ApJ, 549, L51

Kauffmann, G. et al 2003a, MNRAS, 341, 43

Kauffmann, G. et al 2003b, MNRAS, 341, 33

Keel, W.C. 1996, PASP, 108, 917

Joguet, B., Kunth, D., Melnick, J., Terlevich, R., Terlevich, E. 2001, A&A, 380, 19

Maoz, D., Koratkar, A., Shields, J. C., Ho, L. C., Filippenko, A. V., Sternberg, A. 1998, AJ, 116, 55

Nagar, N. M., Falcke, H., Wilson, A. S., Ho, L. C. 2000, ApJ, 542, 186

Pérez, E., Márquez, I., Marrero, I., Durret, F., González Delgado, R. M., Masegosa, J., Maza, J., Moles, M. 2000, A&A, 353, 893

Pindao, M., Schaerer, D., González-Delgado, R. M. & Stasińska, G. 2002, A&A, 394, 443

Raimann, D., Storchi-Bergmann, T., Bica, E., Melnick, J., Schmitt, H 2000, MNRAS, 316, 559

Raimann, D., Storchi-Bergmann, T., González Delgado, R. M., Cid Fernandes, R., Heckman, T., Leitherer, C., Schimitt, H. 2003, MNRAS, 339, 772

Ronen, S., Aragon-Salamanca, A. & Lahav, O. 1999, MNRAS, 303, 248

Schaerer, D., Contini, T, Kunth, D. 1999, A&A, 341, 339

Schaerer, D., Contini, T, Pindao, M. 1999, A&AS, 136, 35

Schlegel, D. J., Finkbeiner, D. P. & Davis, M. 1998, 500, 525

Schmidt, A. A., Coppeti, M. V. F., Alloin, D. & Jablonka, P. 1991, MNRAS, 249, 766

Schmitt, H. R., Storchi-Bergmann, T. & Cid Fernandes, R.1999, MNRAS, 303, 173

Shields, J. C. 1992, ApJ, 399, 27

Sodré, L. & Cuevas, H. 1997, MNRAS, 287, 137

Stasińska, G., Schaerer, D., & Leitherer, C. 2001, A&A, 370, 1

Stasińska, G., Izotov, Y. 2003, A&A, 397, 71

Storchi-Bergmann, T., Eracleous, M., Livio, M., Wilson, A.S., Filippenko, A. V., Halpern, J.P. 1995, ApJ, 443, 617

Storchi-Bergmann, T., Fernandes, R. C. & Schimitt, H. R. 1998, ApJ, 501, 94

Storchi-Bergmann, T., Raimann, D., Bica, E. L. D., Fraquelli, H. A. 2000, ApJ, 544, 747

Taniguchi, Y., Shioya, Y. & Murayama, T. 2000, AJ, 120, 1265

Terashima, Y. et al. 2000, ApJ, 533, 729

Worthey, G. 1992, Ph.D. thesis, Univ. of California, Santa Cruz

Worthey, G. & Ottaviani, D. L. 1997, ApJS, 111, 377